MSc Thesis

Evaluation of Shear Properties of Hydrogel – Thermoplastic Based Tissue Equivalents for Articular Cartilage

Shaiv Parikh
MSc Biomedical Engineering
Delft University of Technology

Supervisors:
Mylene de Ruijter
Dr. Ing. Miguel Castilho
Dr. Jie Zhou

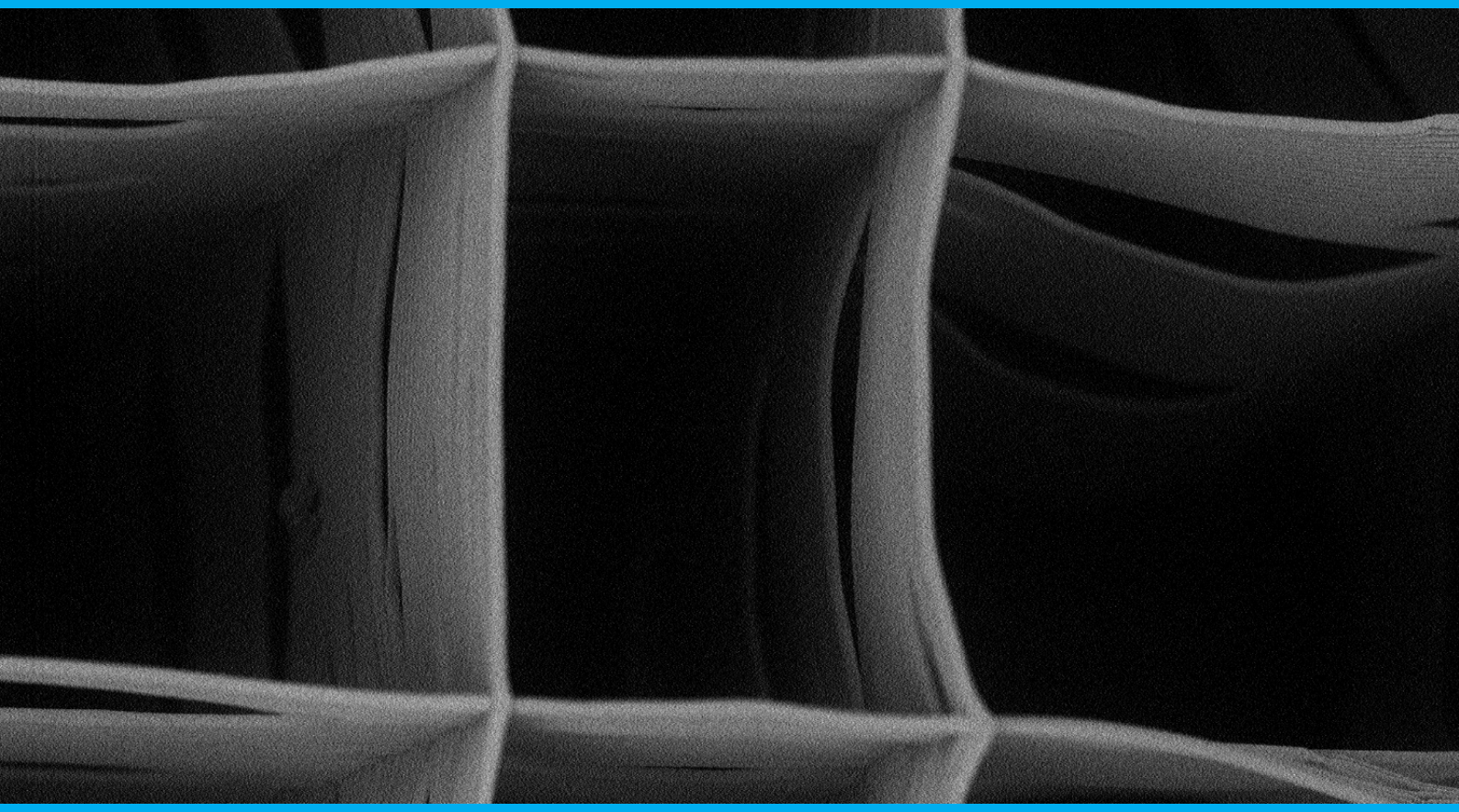

TU Delft

UMC Utrecht

Table of Contents

Abstract

Composite constructs made from gelatin methylacrylamide (gelMA) and polycaprolactone (PCL) have been proven as promising materials to form tissue equivalents which can be used to alleviate the problems arising due to damage of articular cartilage. Despite exhibiting an increase of compressive stiffness (up to 54 - fold) by synergistic combination of the two materials, as compared to gelMA or PCL fiber scaffolds alone, determination of shear properties of the composite construct remains unprecedented. The current study was aimed to comprehend the shear properties of the tissue equivalents made from gelMA or PCL fiber scaffolds. Direct shear tests were performed on composite constructs made from gelMA and boxed architecture of PCL fiber scaffolds with different fiber spacings to generate a comparative basis for shear modulus followed by computational modeling and analysis of the constructs to obtain a better understanding of reinforcing effect of PCL fiber scaffolds in gelMA and validate the experimental results computationally. Results indicate that shear stiffness of the tissue equivalent is dominated by the membrane elements of the boxed architecture of PCL fiber scaffolds which are produced by melt electrowriting (MEW). An association of increase in shear stiffness with decrease in fiber spacing for a given architecture has been depicted.

CHAPTER 1

1.1 Introduction

Acute and chronic degeneration of tissues is one of the major causes of morbidity and mortality in human beings. Some of the cells of our body have the ability to repair certain tissues such as skin and bones . However, such cells eventually succumb to the effects of ageing or trauma [1]. Cartilage is one of those tissues which has limited healing capacities. This is predominantly due to lack of vasculature [2]. A full thickness injury to the cartilage will initiate a healing response with hematoma, mesenchymal stem cell migration and vascular ingrowth [3]. This will result in introduction of collagen type-I instead of collagen type-II and formation of a fibrous tissue with compromised mechanical properties as compared to the uninjured tissue [3]. Partial thickness defects are also observed, which heal even more poorly as compared to full thickness defects [2]. These defects resulting from trauma cause deterioration of quality of life due to prevalence of acute pain followed by limitation in movement [4].

One common approach to alleviate the problems which arise due to damage and loss of cartilage is total joint replacement surgery, however , over time revision surgeries are required which are highly invasive, complicated and expensive [5]. Additionally, revision surgeries can only be done a limited number of times and with the increasing life span the need for undergoing multiple revision surgeries may increase. Hence, a major challenge lies to facilitate the function of chondrocytes along with growth factors and production and survival of the matrix of the tissue in order to regain its original properties [3]. Some techniques such as Autologous Chondrocyte Implantation (ACI) or creating microfracture have accomplished stimulating fibrous cartilage formation but are not so successful due to the diminished mechanical properties of the tissue formed by these techniques when compared to the native tissue. Therefore, one of the potential solutions to this problem can be tissue engineering (TE). TE aims to restore the function of the tissue through delivery of living elements which become integrated into the patient. For this, most investigators rely on the technique of combining cells with matrices [6]. Composite constructs which are made from hydrogel gelatin methacrylamide (gelMA) and thermoplastic polycaprolactone (PCL) are promising candidates to form the tissue equivalents of articular cartilage and help overcome the problems existing with the aforementioned techniques. The choice of the hydrogel gelMA has been made due to its ability to encapsulate cells, provide cell viability and bioresorb in a controlled manner [7]. Whereas, PCL is a medical grade polymer which degrades into non-toxic components and can be printed using additive manufacturing techniques such as melt electrospinning writing (MEW) into highly reproducible fibers at micrometer scale which can be potential candidates to mimic the properties of collagen fibrils [8].

1.2 Articular Cartilage

1.2.1 Structure of articular cartilage

Articular cartilage is a layer of hyaline cartilage which covers the articulating surfaces of the bones , usually ranging from 0.5 to 5 mm in thickness (in the human knee, its mean thickness is ranging from 1.69 to 2.55 mm [9]) and is devoid of any blood vessels or nerves [10]. **Table 1** depicts the average articular cartilage thickness in the major joints of lower limb i.e. ankle, knee and hip. It consists of 4 main components namely- chondrocytes (less than 10%), water (∼70%), collagen (∼20%) and proteoglycans (∼10%). The predominant type of collagen is type-II collagen. The specific architecture of articular cartilage is imperative for bearing the mechanical loads.

Table 1

Average thickness of articular cartilage - ankle, knee and hip joints [11]

Ankle	Knee	Hip
1 to 1.30 mm	1.69 to 2.55 mm	1.35 to 2.0 mm

Articular cartilage is strong in compression as collagen fibers counterbalance the swelling pressure that is built up by the negatively charged proteoglycans that attract water [12]. The organizational structure of the cartilage varies according to its depth. There are three distinct zones with differing collagen fibrils orientation resulting in varying stiffness with each zone [13] . The boundary between the calcified cartilage and zone-III is marked by tidemark (**Fig.1**) . The first zone is the superficial zone (zone-I), followed by transitional zone (zone-II) and deep zone (zone-III). The collagen fibrils are oriented parallel to the surface in zone-I whereas they are perpendicular to the surface in zone-III. The collagen fibrils are obliquely organized in zone-II [14]. A characteristic load - resisting mechanism is observed in uninjured cartilage.

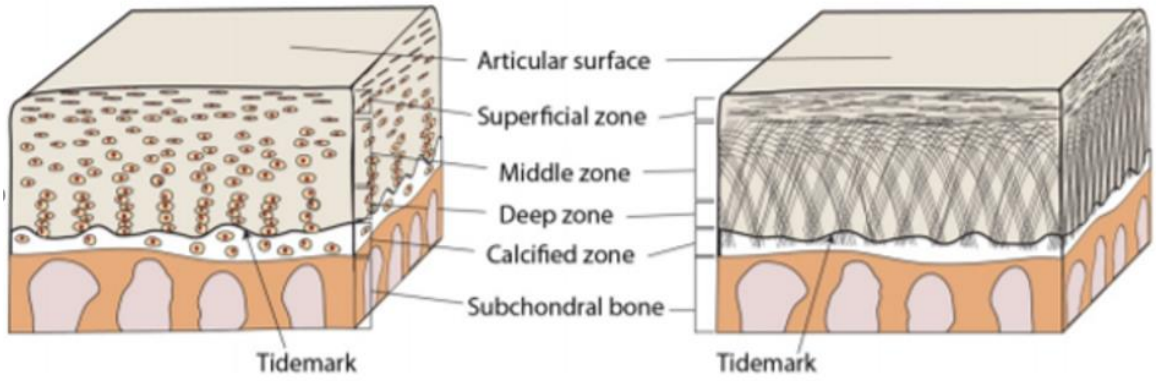

Fig. 1 Schematic representation of zonal architecture of articular cartilage [15]

1.2.2 Load - resisting mechanism of articular cartilage

During normal articulation, the joint forces in the knee on the articular cartilage can mainly be divided into two types, namely compression and shear [16]. Even though, compressive loads are predominant, the tissue must also be able to withstand shear forces [16,17] . The shear force is applied due to the presence of moment during movement, which causes sliding of two opposing articular surfaces **(Fig. 2)**. **Table 2** describes the average shear force distribution in the tibiofemoral joint of a healthy adult during certain activities. The shear forces were derived by decomposing the Contact Forces (CFs). CFs were calculated from contact pressure and contact area derived from the validated knee model with 6 degrees of freedom (DOF) for the patellofemoral and tibiofemoral joints [18].

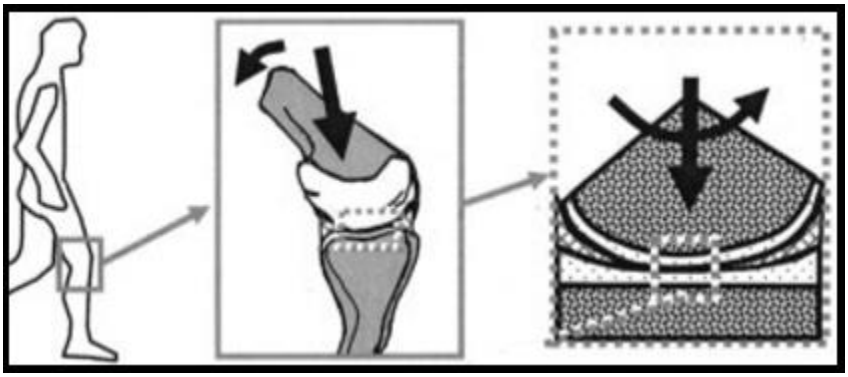

Fig. 2 Schematic representation of joint movement of the knee [17]

The presence of glycosaminoglycans (GAGs) which are attached to the proteoglycans are negatively charged and attract water, which results in osmotic swelling. The swelling is in turn restricted by the tension produced in collagen fibrils. Thus, the resistance to compressive loads is offered by this swollen tissue in the form of fluid pressurization [19]. Compression is not resisted by collagen fibrils directly due to compromised strength owing to slenderness. However, they possess significant tensile strength. The highest tensile strength and stiffness are therefore found in superficial layer where the collagen fibrils are dense and arranged parallel to the articulating surface [14].

Table 2

Average shear force distribution over medial and lateral tibiofemoral compartments. Abbreviation : BW, body weight [18]

Action	Medial	Lateral
Stand – up	0.900 x BW	0.125 x BW
Sit - down	0.075 x BW	0.140 x BW
Squat	0.150 x BW	0.240 x BW
Gait	0.2100 x BW	0.110 x BW
Stair ascent	0.200 x BW	0.125 x BW
Stair descent	0.240 x BW	0.125 x BW

The responses of articular cartilage can be classified as flow-dependent and flow-independent responses. The flow-dependent response occurs due to the movement of interstitial fluid through the matrix due to dilatation of the tissue, which helps in dissipating energy due to frictional resistance. On the other hand, flow-independent response is the resistance offered by cartilage matrix only [17,20,10-25]. Since, simple shear deformation does not give rise to volumetric deformation, the mechanical response observed is flow-independent. As collagen fibers assist in resisting tension more than compression [14], the flow-independent shear rigidity of cartilage is derived from the presence of collagen fibrils [20]. This is because the shear force acting on the cartilage invariably translates to stretching force. **Fig. 3** gives a better representation of the translation of shear force to stretching along the diagonal.

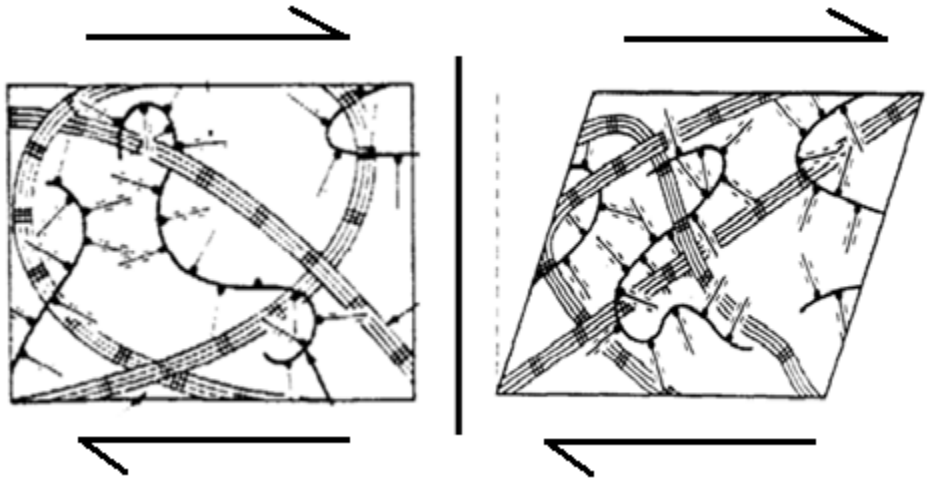

(a) **(b)**

Fig. 3 Schematic representation of (a) Undeformed unit block of cartilage (b) Deformed unit block of cartilage under the influence of shear force [20]

1.3 State of the art

Extensive studies have been conducted on the compressive properties of cartilage, but shear properties of the cartilage need further attention [17]. Conforming to this scenario, TE fiber/hydrogel constructs have been studied mainly for their compressive properties [26-29] . To enable the process of improvement of mechanical properties, studies conclude that it becomes important to understand the reinforcing effect of the scaffold in the hydrogel which increases the synergistic stiffness by 54-fold as compared to just hydrogel or scaffold [26,27,30].

The composite constructs made from gelMA and thermoplastic PCL exhibit a mechanical response on similar lines to that of native cartilage. Gradually decreasing the porosity of the PCL fiber scaffold, thereby increasing the volume fraction of the fibers embedded in hydrogel has shown to increase the slope of stress vs. strain curves **(Fig. 4),** indicating an increase in stiffness of the constructs. The increase in stiffness of the constructs is owing to the reinforcement mechanism exhibited by PCL fiber scaffolds embedded in gelMA [26,29]. Increase in volume fraction of PCL material is proportional to decrease in porosity. Due to higher volume fraction, greater resistance to compressive deformation has been observed in composite gels [26,29], thereby leading to higher stiffness of the tissue equivalents. Despite promising results shown by majorly used "wood-pile"/boxed architecture **(Fig. 5)** of PCL scaffolds embedded in hydrogel in compression [26], its behavior under shear loading is yet to be found out.

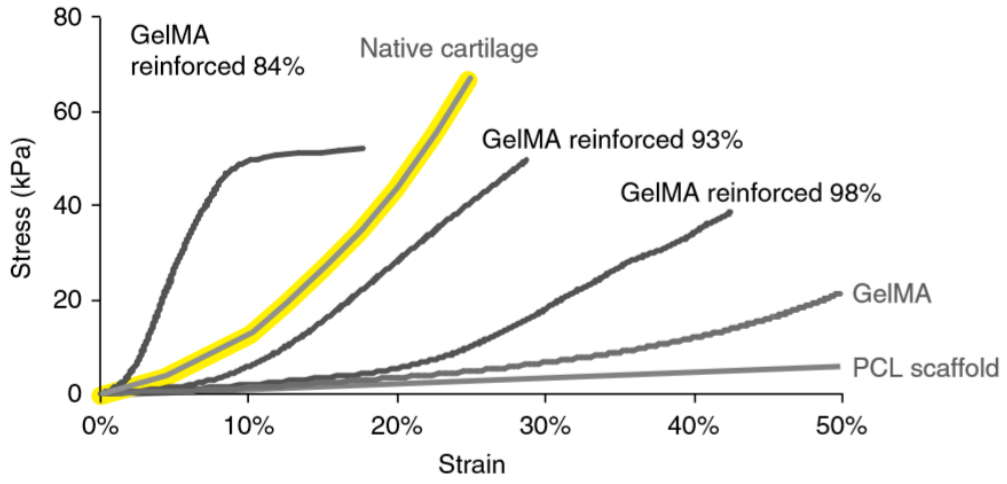

Fig.4 Comparative stress vs. strain curves for native cartilage, PCL scaffold, gelMA and gelMA reinforced with PCL scaffold with different porosities (reinforced _% indicates the percentage of porosity) [26]

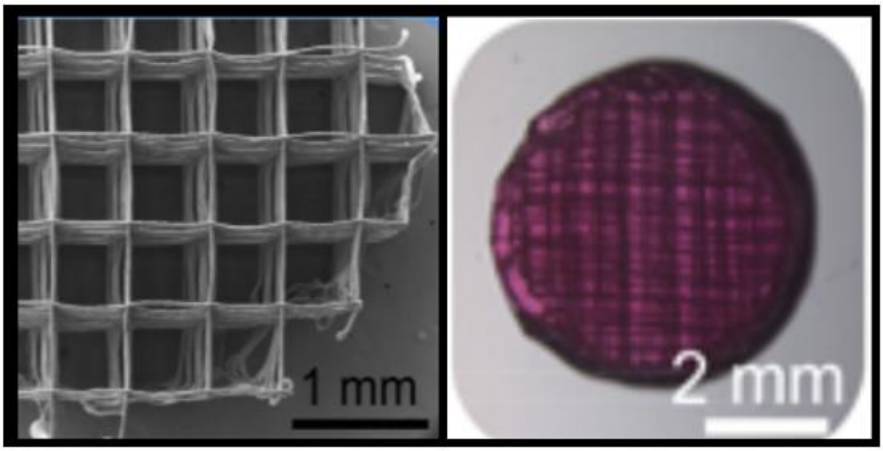

Fig.5 (a) Boxed architecture of MEW PCL scaffold (b) Boxed architecture scaffold embedded in hydrogel [29]

1.4 Insights from previous studies

1.4.1 Experimental methods to determine shear properties of articular cartilage and results

As mentioned earlier, cartilage resists deformation by stretching of the collagen fibers. In case of simple shear, there is no volumetric strain and therefore there is no pressure gradient which will give rise to fluid flow. The use of indentation tests was the most common method for determining the material properties of articular cartilage. Due to difficulties faced in obtaining valid material properties, investigators have moved to the method of applying defined stress fields [21].

Hayes and Mockros [25] have performed their experiments to study the shear properties on cylindrical pieces of cartilage and by fixing the samples to a base and applying torque via a torque applicator (**Fig. 6**). The results yielded two values of shear modulus which consist of short term response and long term response. The short term modulus was found to be 4.1 MPa and the long term modulus which is the asymptotic modulus was found to be 2.6 MPa. The short term response can be considered to be exhibiting linear elastic response as observed in sudden movements. The long term response since it is asymptotic in nature will derive its physical meaning by comparing it to the response derived from sustained loading.

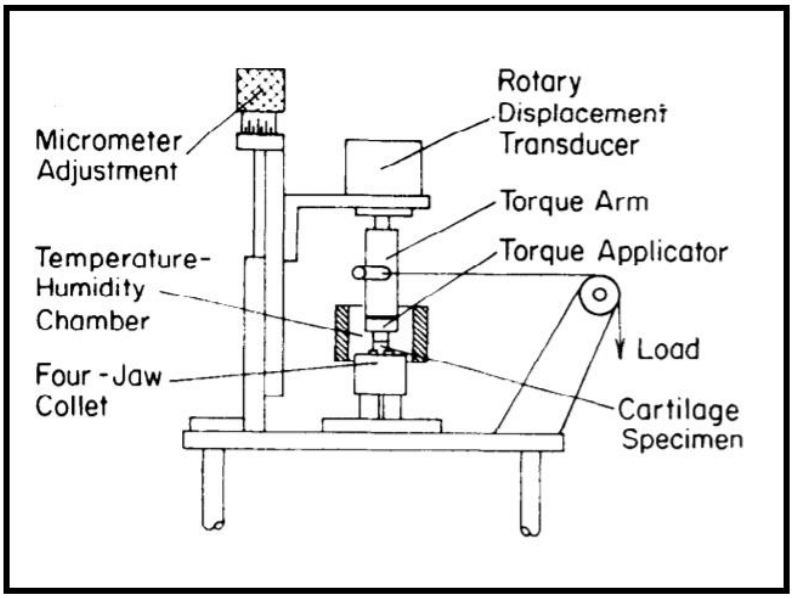

Fig. 6 Schematic representations of experimental apparatus used by Hayes and Mockros [25]

Hayes and Bodine [21] have provided the uncoupled characteristics and the complex shear modulus of an articular cartilage by applying sinusoidal torque loads using a sinusoidal shear generator (**Fig. 7**). The reason for doing this was to understand the phase difference of stress and strain which would further allow calculation of complex moduli. Here too, the experiment was limited to small strains in order to get insights into the properties of solid matrix. To achieve sufficient friction while applying torque, the specimen was compressed by 7% of thickness (0.1 cm). The test was conducted for a fixed amplitude of 30 x 10^{-6} cm / cm, the maximum shear stress that can be generated due to sliding in a human knee is 0.01 MPa which corresponds to strain levels of 0.01 to 0.02. Thus, careful experimentation setup needs to be considered while testing the material properties. The results showed that the short term shear modulus was 1.5 MPa. However, there was no mention about the long term shear modulus.

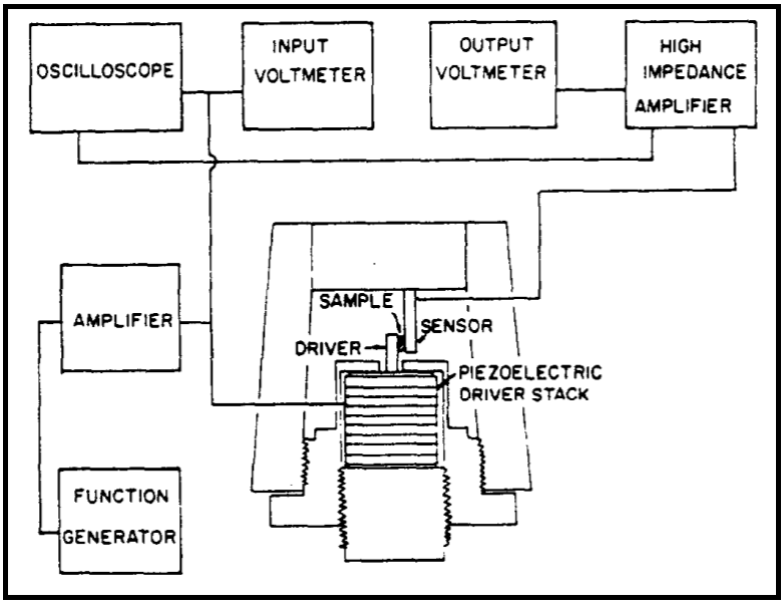

Fig. 7 Schematic representations of shear generator used by Hayes and Bodine [21]

An interesting study was conducted by *Zhu WB et al.*[31] regarding the viscoelastic shear properties of articular cartilage by applying torque loads (**Fig. 8**) with a physiological frequency range of 0.01 – 20 Hz. The effect was also calculated in tandem with applied compressive strains of 5, 9, 12 and 16 %. This is one of the studies in which care was taken to mimic the experimental setup as close to *in vivo* conditions as possible. The compressive strain applied was allowed to relax for 30 - 60 minutes in order to achieve the equilibrium condition. The equilibrium compressive modulus was obtained as 0.31 $\pm$ 0.09 MPa and the dynamic shear modulus was found to be 1.51 $\pm$ 0.37 MPa. These values were the highest at 16 % compressive strain with frequency of 1 Hz. It is to be observed in this study that the test was performed to determine the dynamic shear properties and application of infinitesimal shear strains were applied in order to avoid the flow of interstitial fluids.

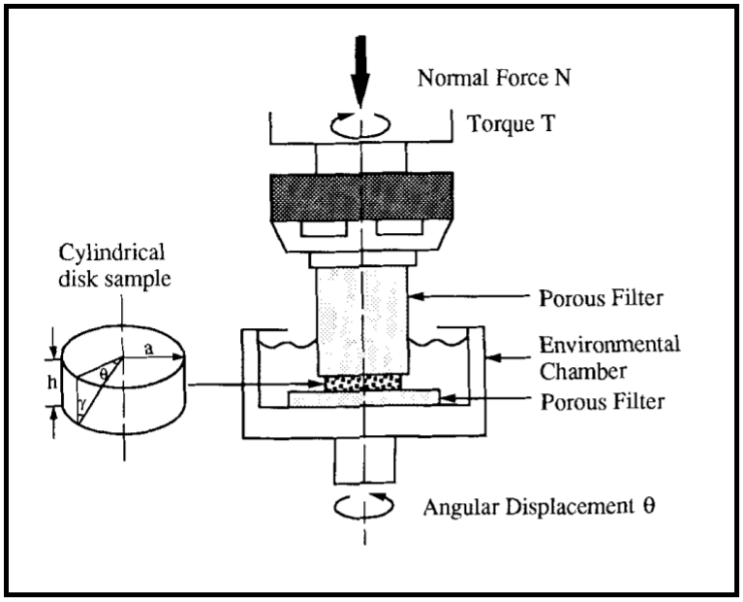

Fig. 8 Schematic representations of experimental apparatus used by Zhu WB et al. [31]

Compared to most of the aforementioned studies, the study performed by *Spirt et al.*[23] showed interesting results for strain - dependent intrinsic viscoelastic properties of articular cartilage. Four different shear strains ranging from 3 – 16 % were applied on the specimen using a materials testing machine (**Fig. 9**) and the corresponding stresses were calculated after allowing a relaxation period of about 15 minutes. It was found that the equilibrated stresses and strains varied in a linear fashion **(Fig. 10)** with the mean equilibrium shear modulus found as 0.37 ± 0.14 MPa . This kind of result has the capacity to be proven useful in the numerical modelling aspect since it has a direct relation of stress and strain. The only challenge for application of this result in a simplified numerical model will be to consider the effect of relaxation period before considering the direct relationship of stresses and strains.

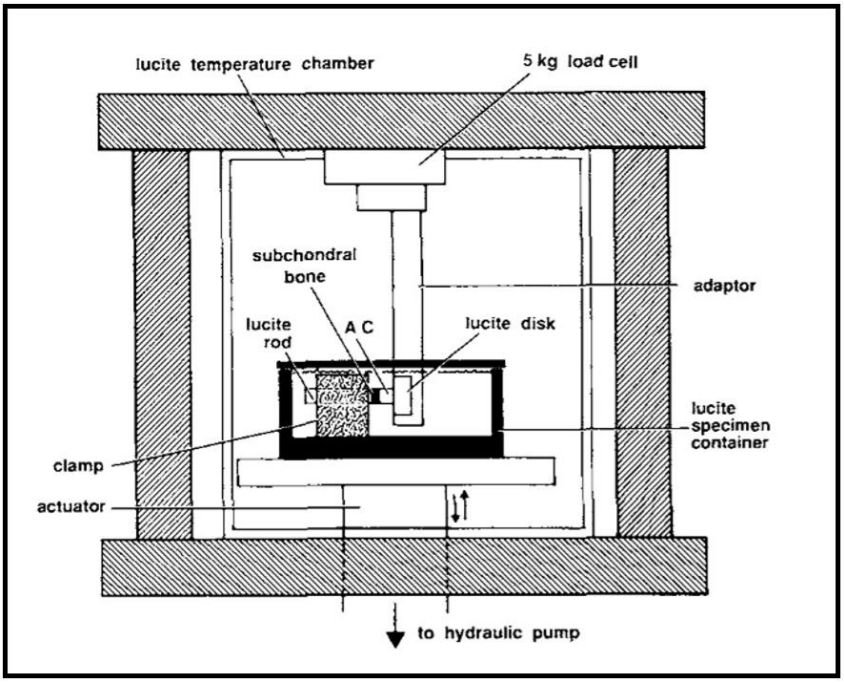

Fig. 9 Schematic representations of experimental apparatus used by Spirt et al. [23]

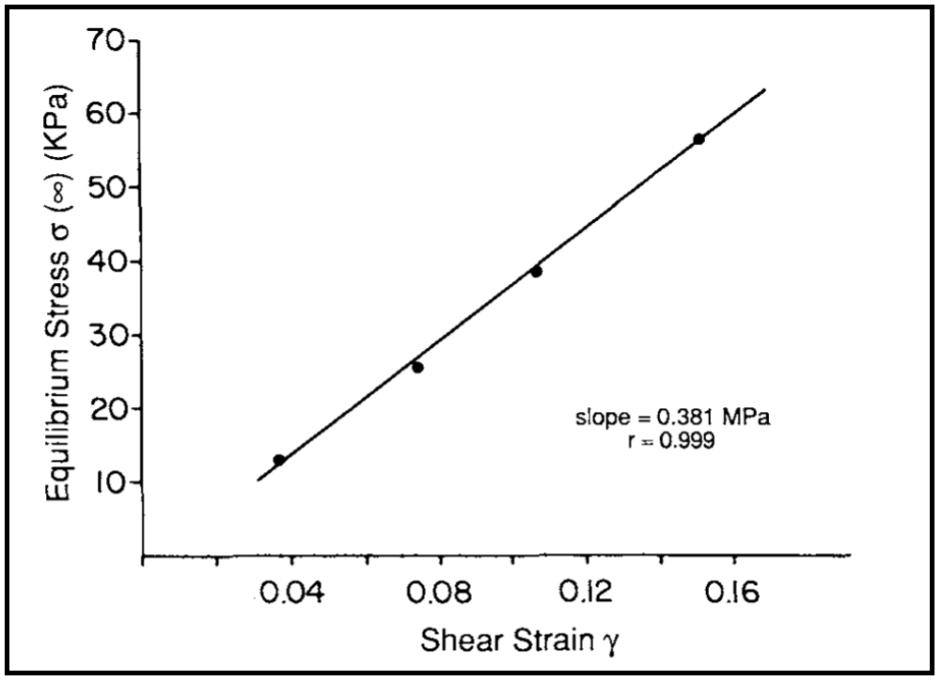

Fig.10 Equilibrium stresses vs. strain graphs [23]

A study by *Wong et al.* [17] elucidated the effect of lubrication and degeneration on shear deformation of articular cartilage. To do that, shear tests were performed on the articular cartilage samples replicating knee joint movement by placing two samples of cartilage adjacent to each other but on the opposite face **(Fig. 11)**. Also a pre-compressive load was applied to enable proper friction between two sliding samples. The effect of lubrication was checked by using two different lubricants namely Synovial Fluid (SF) and Phosphate Buffered Saline (PBS). Also, the focus of the study was to highlight the depth - dependent material properties under shear deformation. The shear modulus of a normal tissue with SF as lubricant was found maximum at the surface (0.056 MPa) and decreased with depth with an average of 0.028 MPa. The overall shear modulus was found to be in the range 0.26 - 0.32 MPa. The shear strains were calculated on observing and measuring the displacement of the fiducial markers in the cartilage before and after deformation. This study proves to be important from numerical modelling point of view since the testing is done without considering the viscoelastic effects and only the linear elastic material properties are obtained. It is to be noted that most of the studies delineated above have been conducted either on bovine articular cartilage except for *Hayes and Mockros* [25] and *Wong et al.* [17] which used human cartilage samples (**Table 3**).

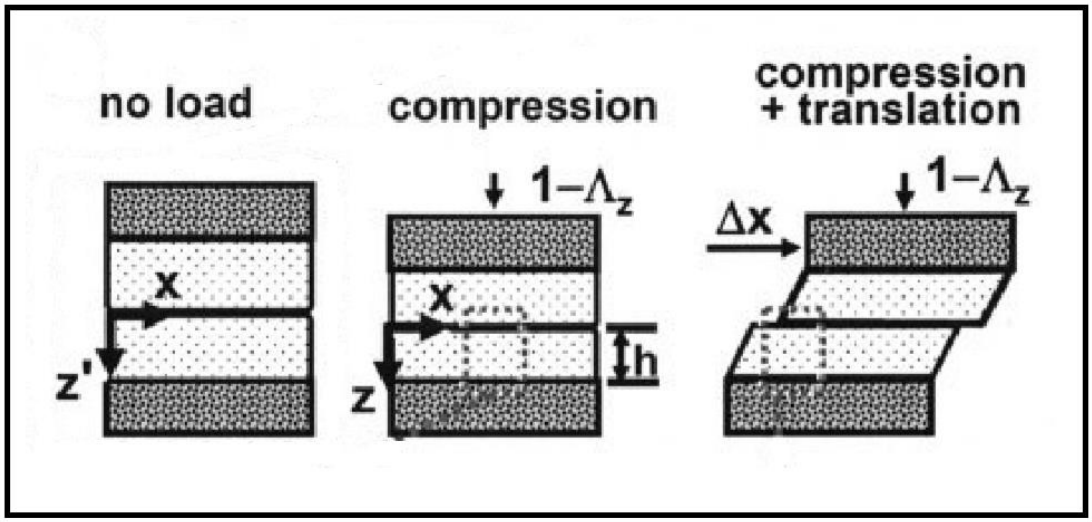

Fig. 11 Schematic representation of shear test setup [17]

Table 3

Details of shear moduli obtained from different studies

Studies	Type of Shear Modulii	Values (MPa)	Origin of Cartilage (knee joint)	Reference number
Hayes and Mockros	Short term and Long term (equilibrium)	4.1 and 2.6 (respectively)	Human	25
Hayes and Bodine	Short term	1.5	Bovine	21
Zhu WB et al.	Dynamic	1.51 ± 0.37	Bovine	31
Spirt et al.	Equilibrium	0.37 ± 0.14	Bovine	23
Wong et al.	Linear elastic	0.26-0.32	Human	17

1.4.2 Experimental characterization of shear properties of tissue engineered constructs

Cell-polymer constructs have been characterized to have the potential to repair defects in cartilage which has limited regenerative capacity due to lack of proliferative capacity from surrounding cells [6,32,33]. Numerous studies have been performed to test the effects of these cell laden tissue-engineered constructs. Mechanical properties of these constructs holds significance as much as its capacity to enable cell viability.

Stading and Langer [33] have demonstrated the biomechanical properties and the effect of build-up of ECM in cell laden polymer scaffold made from polyglycolic acid (PGA) under shear loading. The constructs were made by extruding 12 mm diameter of PGA fibers into cylindrical scaffolds with 1 cm diameter and 0.2 cm thickness. The scaffolds were further attached with chondrocytes by pre-wetting in well dishes (coated with 1% agarose) containing medium with cells and placing them on orbital shaker at 75 rpm for 3 days. The constructs were then transferred to new dishes (not coated with agarose) and placed on a 50 rpm orbital shaker for 8 weeks. The medium was replaced every 2 – 3 days. The cylindrical samples of scaffolds were placed in sinusoidal torque applicators with a frequency range of 0.001 - 5 Hz. A typical illustration of torsional load application on tissue engineered constructs can be seen in **Fig.12**. The maximum shear strain, which occurs at the boundary of the specimen, was reported as 5×10^{-4}. The complex shear modulus (G*) was calculated from the given value of strain. A pre-compressive load which, after relaxation, gave 5 % axial strain, was also applied in order to achieve adequate friction. It was observed that under the application of these loads, the diameter of the construct increased and the relation was found to $G^* \propto d^4$ (d is the diameter of the construct) and G* was compensated accordingly. The complex shear modulus G* comprises of the storage modulus (G') and loss modulus (G''). The G' part of G* indicates the energy stored in the material due to deformation

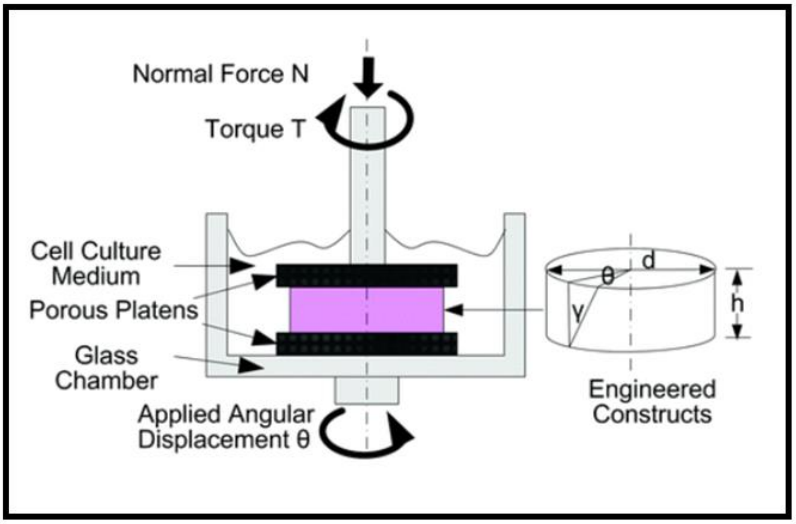

Fig. 12 A typical schematic representation of rotational force applicator on engineered constructs [34]

which is generally done by the elastic component of the material. The results depicted that the initial presence of G' was simply due to PGA fibers while the cells had just been seeded in the scaffold and there was no formation of ECM. With passing of days, the PGA mesh depleted due to its bioresorbable nature and the G' part of the scaffold dropped to zero. But as the cells started creating ECM, G' started to rise again **(Fig. 13)**. The important conclusion from this study was that a continuous spanning of fibers in the construct , be it PGA fibers or collagen-GAG network from secreted ECM, governed the shear deformation of the construct even though the material properties did not reach those of a native cartilage.

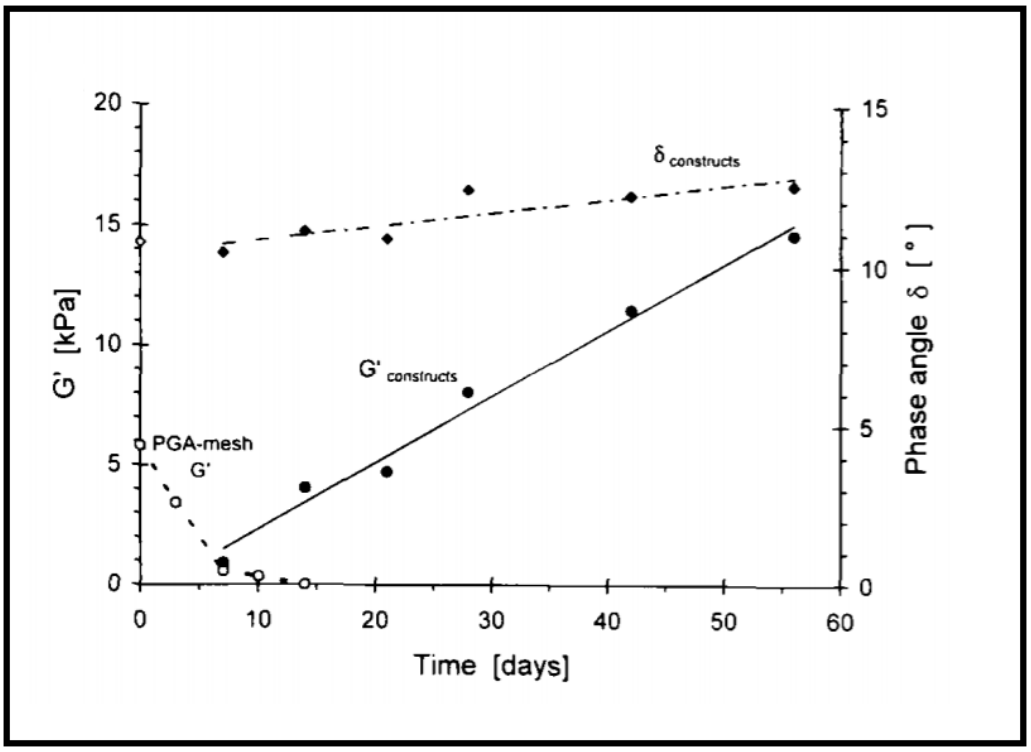

Fig.13 G' vs. time graph [33]

Wan et al. [34] have presented in their study the viscoelastic property of chondrocyte laden low-viscosity alginate scaffold under torsional loading. The purpose of the study was to correlate the scaffold stiffness with cell culturing time and cell density. In contrast to the study by *Stading and Langer* [33], this study concluded that the stiffness of the scaffold in shear is derived not due to strong presence of collagen but instead due to presence of glycosaminoglycans. The equilibrium shear modulus of acellular alginate hydrogel was found to be approximately 1 kPa. The magnitude of the scaffold increased to 12 kPa when seeded with chondrocytes in the concentration 60 M/ml and cultured for 40 days. The study also concluded that a better understanding of detecting changes in the cell- seeded hydrogels was derived from shear tests instead of compressive tests.

Stammen et al. [35] have studied the mechanical properties on polyvinyl alcohol (PVA) gels under the effect of direct shear and unconfined compression. The commercial name for the PVA hydrogel used was Salubria ™. The study was carried out to characterize the mechanical response of two different formulations of the hydrogel. Formulation A had 75 % water content while formulation B had 80 %. The mechanical response was studied for different compressive strain rates of 100 % min^{-1} to 1000 % min^{-1} and shear strain rates were 75 % min^{-1} to 750 % min^{-1} . The strain rates showed significant difference in compressive modulus for formulations A and B while

the shear modulus lied consistently between 0.01 MPa at 10 % strain and 0.45 MPa at 60 % strain for both strain rates. Hence, it was concluded here that the intrinsic solid matrix was mainly responsible for shear strength.

Boere et al. [36] have demonstrated in their study the effect of covalent bonding of PCL with hydrogel gelMA under mechanical loading. Three study groups were considered out of which two represented different blends with PCL. One of was poly(hydroxymethylglycolide-co-ε-caprolactone) / poly(ε-caprolactone) (pHMGCL/PCL) and the other was pHMGCL/PCL functionalized with methacrylate groups (pMHMGCL/PCL). The third group was hydrogel only without reinforcement. Apart from compression tests, the samples were also subjected to rotational forces in order to check the effect of reinforcement which is usually through the bonding between the hydrogel and the fibers. The samples were subjected to 20 N of compressive load and then 100 cycles of rotational force in a rheometer. It was found that the pHMGCL/PCL construct showed lack of recovery after loading was removed while pMHMGCL/PCL constructs retained their shape. The gelMA had disintegrated completely. The important result found here was the shape retention and residual strength left after the experiment. No shear strength parameters were achieved in this study but it gives insight into the importance of reinforcement mechanism in order to achieve higher strengths.

Moutus et al. [37] have described a novel method of reinforcing cartilage derived matrix (CDM) with PCL fibers and the advantages encountered due to this procedure. Three groups comprised of CDM, fiber reinforced (FR) CDM and PCL scaffolds were formed and seeded with ASCs to perform experiments at different time points. The CDM scaffolds were prepared from full thickness porcine cartilage from healthy femoral condyles. The cartilage was minced and put in distilled water (concentration 0.1 $g.ml^{-1}$) and then homogenized using a tissue homogenizer. The cartilage slurry was then pipetted in a well plate (4ml/well) and frozen overnight at - 80 ^{o}C. 6 mm diameter biopsy punches were used to cut samples with 2 mm thickness. The PCL scaffolds were produced using a custom-built miniature weaving loom. 156 µm diameter multifilament yarns were used to produce the scaffold. The FR CDM scaffolds were made by spreading the cartilage slurry on the PCL scaffold, ensuring all the pores of the scaffold were filled with slurry and then freezing the scaffolds covered in slurry overnight at - 80 ^{o}C. 6 mm biopsy punches were used to cut out the samples after 24 hours. The complex shear modulus was examined by performing dynamic frequency sweeps at a strain amplitude of 0.05 and frequencies having a range 1 to 50 rad. s^{-1}. PCL showed the highest complex shear modulus at all time points. The results yielded at frequency 10 rad/s for PCL constructs showed a maximum value of complex modulus at 28 days of culture while it decreased on day 42 with the lowest being at day 1 followed by day 14. The loss angle was also observed to be the minimum on day 42 for all constructs which indicated the scaffolds losing their viscosity due to ECM deposition by the cells. The results can be observed in **Fig. 14**.This study indicates positive results for PCL reinforced CDM constructs.

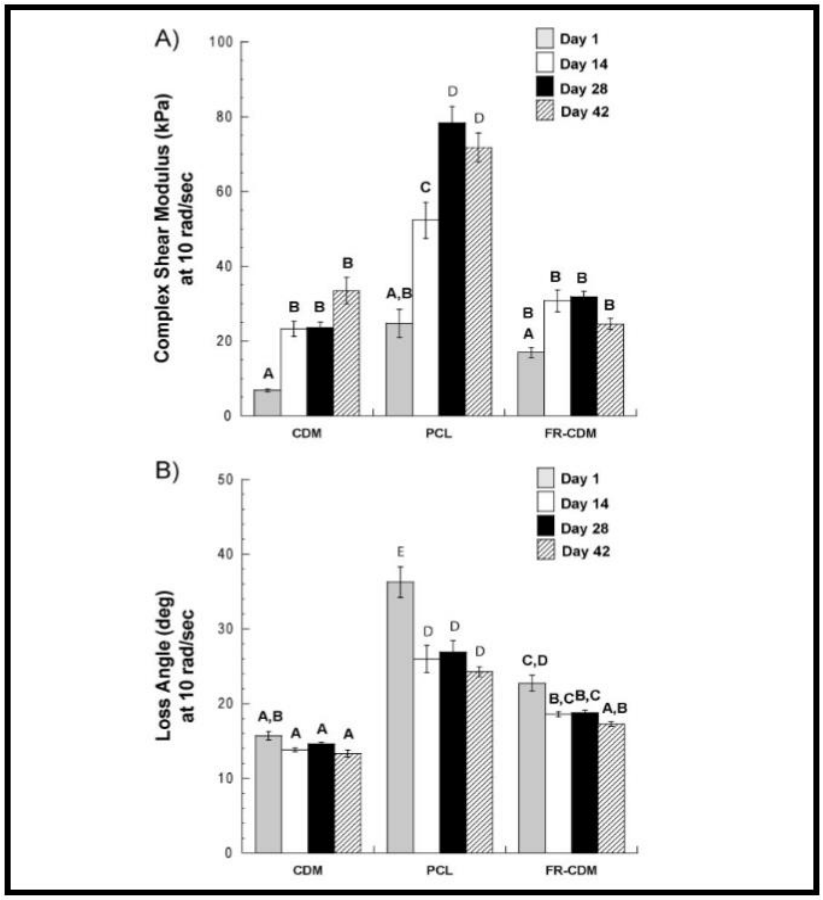

Fig.14 Complex shear moduli and loss angle for CDM, PCL and FR-CDM constructs at time points 1,14,28 and 42 days using dynamic shear testing using strain amplitude as 0.05 and frequency of sweep as 10 rad/s [37].

1.4.3 Computational methods to determine mechanical properties of tissue engineered constructs

Attempts have been made to capture the stress distribution and deformation of collagen fibrils of cartilage by using numerical models [38-40]. These models ([38-40]) usually consider biphasic nature of articular cartilage consisting of solid matrix (proteoglycans and collagen fibrils) and liquid phase [38]. Tissue engineered constructs try to mimic this composition of the cartilage by the recent use of fiber reinforced hydrogels. The fibers reinforcing the hydrogels can be assumed to be playing a role of fibrillar part of the cartilage. Previous studies have tried to reproduce the reinforcing mechanism of fiber reinforced hydrogels by the use of computational models [27, 29] . The aim of doing these studies ([27, 29]) was twofold – to get a better insight into fiber interaction with hydrogel, which would provide a scope for further improvement in mechanical properties and to create a library of constructs with different architectures with predefined mechanical properties. To capture the reinforcing effect of fibers, the models assumed the fibers to be modelled either individually or in combined forms such as laminas, with interconnection

points where overlap of fibers is observed, to be behaving as trusses with a different stiffness of its own (**Fig. 15**). Both the models have a boxed architecture as observed previously.

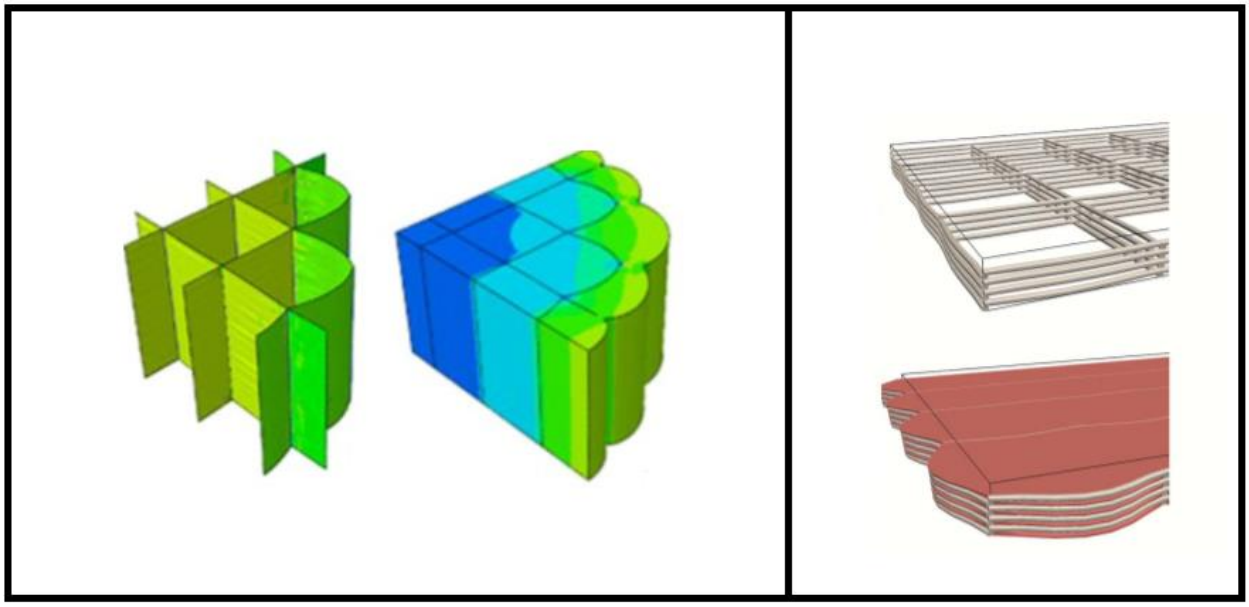

(a) **(b)**

Fig.15 (a) Modelling of scaffold and gel/fiber composite. Here in scaffold, the fibers are assumed to form laminas with the interconnection points behaving as trusses [27]. (b) Modelling of scaffold and gel/fiber composites with fibers modelled individually in the scaffold [29].

However, the numerical models were not able to match the experimental results in terms of mechanical response of the constructs (**Fig. 16**). Homogenization of fiber-reinforced hydrogels has also been performed. However, certain parameters such as sagging of fibers in MEW printed scaffolds and the unreinforced initial layer of hydrogel were not considered during homogenization which led to overly stiff response of the model. Nevertheless, the attempt to homogenize the fiber - reinforced hydrogels forms a decent basis for further modifications [41].

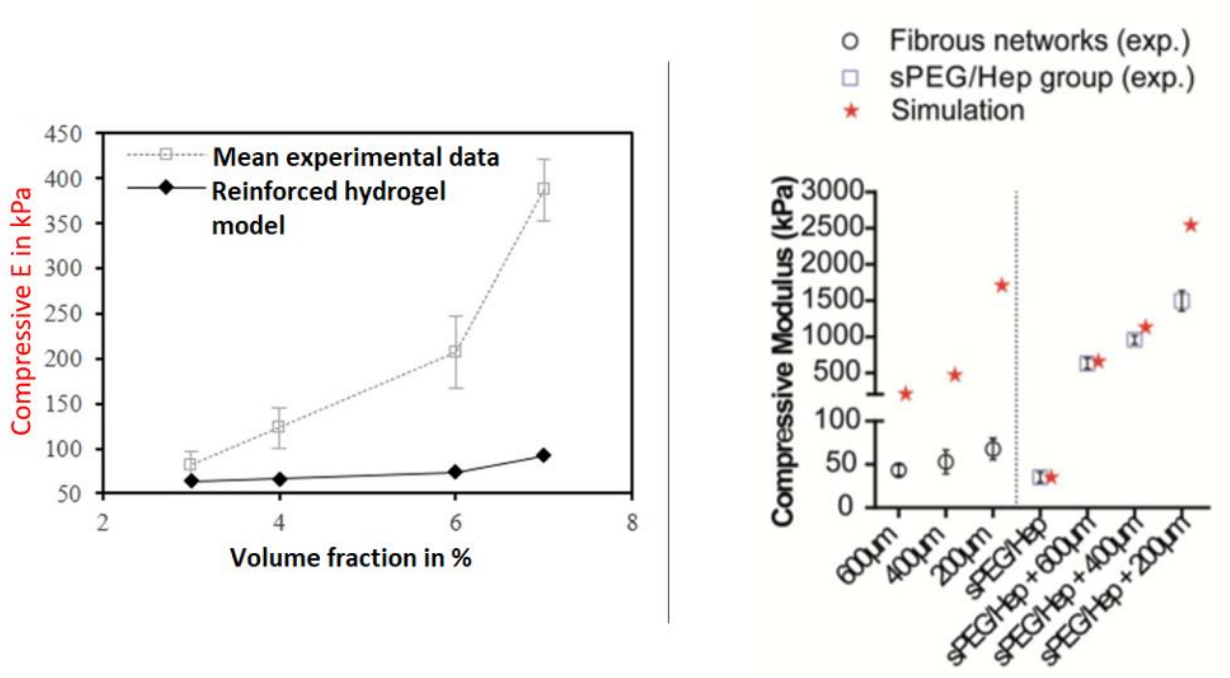

(a) **(b)**

Fig.16 (a) Comparison of experimental and computational results of compressive moduli of gelMA/PCL constructs with different volume fractions of fibers [27] (b) Comparison of experimental and computational results of compressive moduli of PCL fibrous networks, hydrogel sPEG/Hep and combination of hydrogel and PCL [29].

1.5 Discussion of insights from previous studies

To imitate the mechanical behavior of hydrogel-thermoplastic tissue equivalent, it is crucial that the mechanical response of the construct must coincide with articular cartilage. Most of the studies exhibit viscoelastic properties of the articular cartilage. Accepting viscoelasticity will ultimately affect the computational models since it will become important to adopt viscoelastic properties for modelling. This in general will introduce complexities in analyzing the gel - fiber interaction as compared to a simplistic approach of utilizing hyperplastic or linear elastic material properties. This fact was taken into consideration while building the computational models based on compressible hyperplastic (gelMA) and linear elastic scaffold (PCL) [27] or linear elastic gel and linear elastic fibers [28,29] which will further provide a base for analyzing tissue equivalents under shear deformation.

As it is also evident that the aforementioned experiments for articular cartilage and tissue equivalents usually apply torsional shear force under application of pre-compressive loads in order to ensure proper contact between the force applicator and articular cartilage/construct. Only two experiments (*Wong et al.*[17] and *Stammen et al.* [35]) describe the mechanical response

under simple or direct shear. It is to be noted that *Wong et al.* [17] also used pre-compressive loads along with direct shear. Therefore, only *Stammen et al.* [35] produced experimental results based on shear tests without including pre-compressive loads. Such a model will be apt for the current study since, the application of simple shear will provide a better insight into gel – fiber interaction under shear loading and help determine the actual shear modulus of the construct without any pre-compressive loading which will tend to increase the shear modulus of the material. Direct shear force application will also provide a close representation of physiological loading condition *in-vivo* as compared to torsional force application. As far as computational models are concerned, the study of shear deformation on gelMA/PCL scaffold is unprecedented. As previous studies have aimed to study the gel – fiber interaction under compressive loads only.

1.6 Research Questions

It can be concluded from previous studies that there is a scope for improvement in the shear properties of tissue equivalents. It has been observed from experimental results that the mechanical properties have not been able to match the native tissue. This indicates the need to enhance the shear resisting properties of the constructs. Since gelMA and PCL fiber composites have shown promising results in compressive loading condition, a hypothesis can be laid for the composites to exhibit similar behavior under shear deformation. From the computational models that have been prepared mainly for compressive loads, the need is adequately understood for studying the effect of shear loading on a tissue engineered construct. The knowledge of reinforcement mechanism of fibers in hydrogels will enable us to strategize the enhancement of shear property of tissue equivalents in a defined manner.

Considering the above delineated results, following research questions were raised in this study:

1. Does the reinforcement of gelMA with PCL fiber scaffolds exhibit an increase in shear modulus?
2. What is the extend of increase in shear modulus of gelMA due to reinforcement effect of PCL fiber scaffolds?
3. Can computational modeling be used to predict reinforcing effect of PCL fiber scaffolds in gelMA?

CHAPTER 2

2.1 Methods, materials and construct fabrication

2.1.1 PCL fiber scaffolds

PCL fiber scaffolds with a height of 1 mm were printed using MEW (RegenHU 3D Evolution MEW) **(Fig. 17)**. A "boxed type" architecture was printed which involved printing the fibers in a criss-cross fashion **(Fig. 17)**. This resulted in fusion of fibers at junctions encountered at 0^{o} to 90^{o} orientation of fibers. Scaffolds were printed with three different fiber spacings – 200 , 400 and 800 µm. As the height of the scaffold increased, the accuracy of fiber deposition decreased. Hence, the height of the scaffolds was limited to 1000 µm. Different parameters required to control the efficiency of printing were air pressure in the material chamber (0.120 MPa), temperature of the print head (90 ^{o} C), voltage at the nozzle (- 9.5 kV), distance of the nozzle from the collector plate (6 mm) and the relative velocity of the substrate/print head and the jet (15 mm/s).

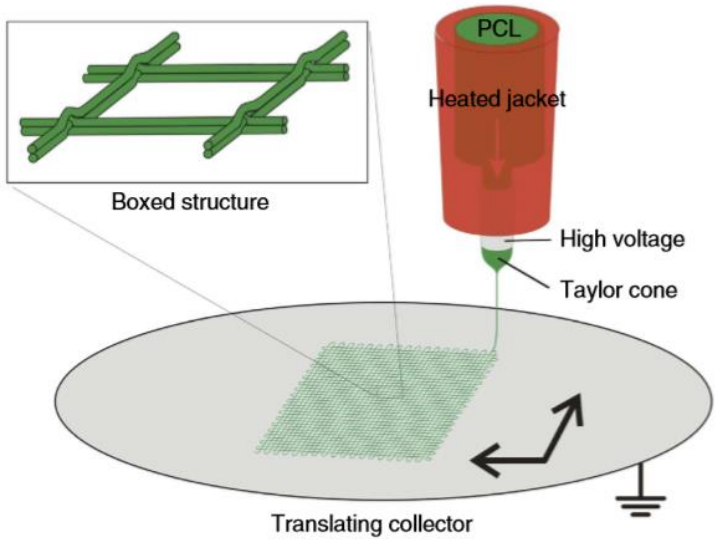

Fig.17 Schematic representation of 3D printing of PCL fibers in Boxed Structure using the MEW technology [26]

2.1.2 Preparation of gelMA

To prepare the hydrogels, the initial step was to prepare gelMA solution. 80% Degree of Functionalization (DoF) non-sterile porcine gelMA was taken. Since only the material properties were to be tested (without addition of cells), preparation of gelMA solution under non-sterile conditions was accepted. A solution of phosphate-buffer saline (PBS) + photoinitiator (PI) Irgacure with concentration 1% w/v was prepared. The PBS + PI solution was added to gelMA such that a 10 % w/v solution of gelMA was obtained. The gelMA solution was then placed in the incubator at 37^{o} C till the gelMA in solid form was homogeneously dissolved.

2.1.3 Preparation of samples

Shear properties of individual PCL fiber scaffolds only, hydrogel, and composites (hydrogel embedded with PCL fibers) were of interest. The PCL fiber scaffolds comprised of samples with fiber spacing of 200 , 400 and 800 µm . The fiber scaffold samples were carefully extracted from an initial bigger fiber mesh (2.4 x 2.4 cm to 3.2 x 3.2 cm) by using a scalpel to cut the meshes in required planar dimensions. The hydrogels and composites were prepared using square shaped (dimensions of each hole being 5 x 5 x 1 mm) teflon mold (**Fig. 18**). Depending on preparation of hydrogels only or composites, the molds were filled with either hydrogel or placed with scaffold first in the hole and then filling up with hydrogel using a gel pipette. A glass slide was put on top of the mold and clamped tightly in order to prevent exposure to oxygen. Then the mold was put in a UV cross-linker (UVP cross-linker series CL-1000 254 nm wavelength) for 15 minutes to achieve cross-linking of gelMA. After cross-linking was achieved, the samples were put in well-plates containing PBS and stored overnight in a fridge. The planar dimensions of all the samples were decided to be taken as 5 x 5 mm whereas the thickness of the samples was decided on the basis of thickness of PCL fiber scaffolds, i.e., 1 mm . 7 samples of each type were prepared, resulting in 49 samples in total.

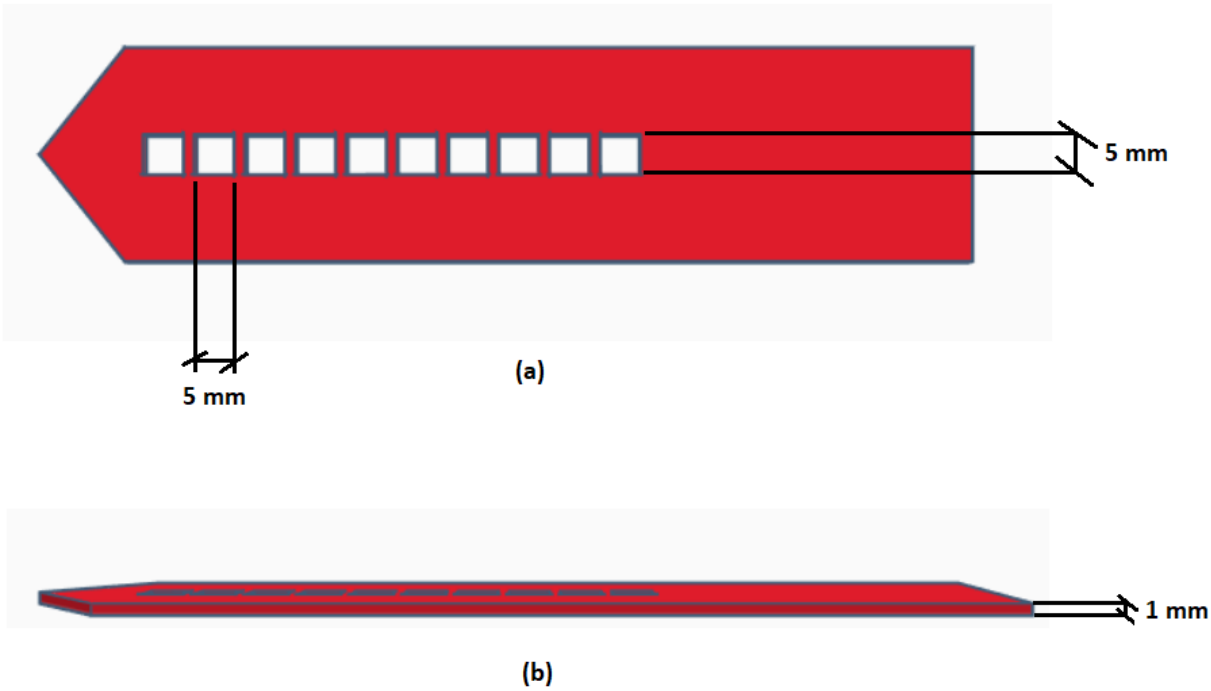

Fig.18 Teflon mold for hydrogel preparation (a) Top view of the mold (b) Front view of the mold

2.2 Experiment

2.2.1 Machine and accessories

Shear tests were performed on Dynamic Mechanical Analyzer (DMA Q800 TA Instruments). Use of Tension Film clamp was made to perform the shear tests. Top and bottom shear plates were designed according to the arrangement of the Tension Film clamp. Shear plates were produced from the material R05 using digital light processing (DLP) 3D printer (EnvisionTEC Perfactory 3D printer). The shear plates were then fixed on the Tension Film clamp of the DMA machine (**Fig. 19**).

2.2.2 Sample fixation and removal

The method for preparing the samples for testing both the categories of samples, i.e. PCL fiber scaffolds only, hydrogel and composites, was identical. Cyanoacrylate glue (ergo.® 5400 kunststoff) was applied in a thin layer to allow only the surfaces of the scaffolds to come in contact with the shear plates. The sample was then placed on the shear plates. It was ensured that both the surfaces of the sample were in contact with the shear plate. After placing the sample, the sample was left there to stabilize for 5 minutes. After the testing was finished, the samples were removed from the shear plates using acetone.

2.2.3 Load Application

Even though a Tension Film clamp was used for load application, the tensile force was converted to a shear force due to the offset provided by the sample between the two shear plates. The offset was equal to the thickness of the sample which was 1 mm. The top shear plate was fixed in its position while the bottom shear plate was allowed to move under the application of force (**Fig. 19(b) & 19(d)**). Since the plates were not aligned in the line of action of force and the sample stuck between the two plates provided an offset to the force, one surface of the sample remained stuck to the top shear plate while the surface attached to the bottom shear plate experienced uniform displacement under the application of force, ultimately giving rise to shear deformation (**Fig.19(c) & 19(e)**). A loading rate of 1 N/min was applied to the sample in order to maintain quasi-static loading condition until the sample failed. A pre-load of 0.05 N was applied in order to remove any misalignment of the shear plates. The application of shear force on samples resulted in force vs. displacement curves. The response of the sample in the range of 0 - 0.1 displacement was desirable. This is due to the fact that the physiological shear loading condition resulted in 0.01 to 0.1 strains [17,30]. Hence, to study the mechanical response of the tissue equivalent, upper limit of strain value (i.e. 0.1) observed under physiological conditions was considered for testing. In our case, the thickness of the sample was 1 mm. Therefore, a deformation of 0.1 mm would result in strain of 0.1. Mean values of either stiffness or shear modulus for the aforementioned range, for 7 samples of each type of fiber scaffold and composite along with hydrogel, were calculated from the experimental results.

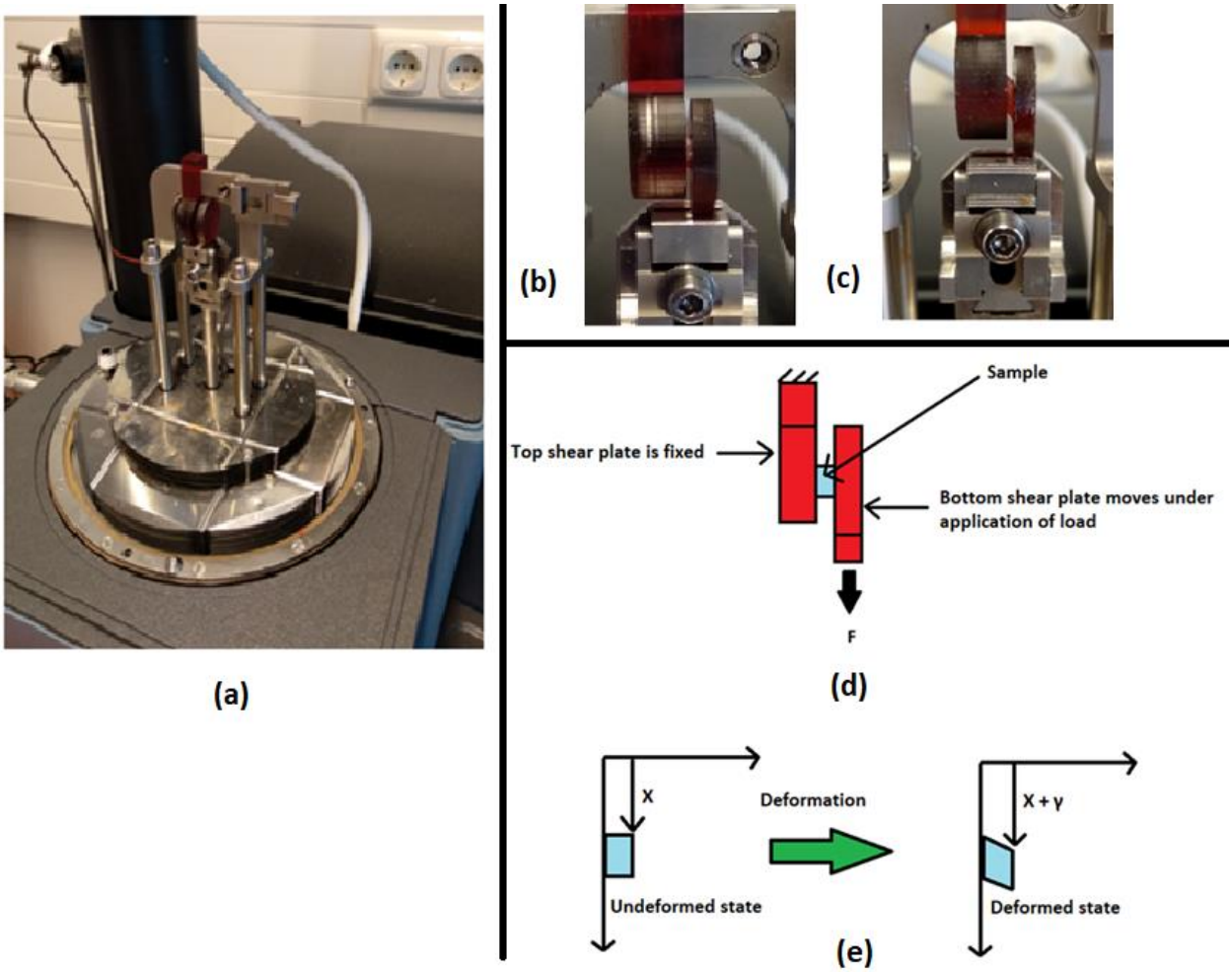

Fig.19 (a) General view of shear plates set up on the Tension Film clamp of Dynamic Mechanical Analyzer (DMA Q800 TA Instruments) (b) Close up front view shear plates and sample in undeformed state under (c) Close up front view shear plates and sample in deformed state under (d) Schematic representation of load application to the sample (e) Schematic representation of shear deformation of sample under shear force (γ is the shear deformation)

2.2.4 Statistical analysis of experimental data

One way ANOVA test and post - hoc Tukey HSD test were performed on the experimental data in order to test the difference between the groups. Fiber scaffolds consisted of 3 groups (consisting of three different spacings) with 7 samples in each group , while, hydrogel and composites consisted of 4 groups with 7 samples in each group.

2.3 Computational Model

Continuum finite element (FE) models were implemented to study the reinforcement mechanism of the fiber scaffolds embedded in hydrogel gelMA. The architecture and modeling strategy was inspired from the previous study performed by *Castilho et. al.* [27] which was aimed to understand the reinforcing effect under compression. Theoretical understanding of the reinforcement effect will provide a basis for more effective designs of architectures of the fiber scaffolds and open up a wide range of applications in the field of tissue engineering (TE).

2.3.1 Modeling Strategy

As described earlier, the hydrogel-thermoplastic composite material was broken down into two parts – PCL fiber scaffolds and hydrogel gelMA. As described in the previous study by *Castilho et. al.* [27] , the fiber scaffold was idealized as unidirectional membrane like elements due to parallel deposition of micro-fibers. Due to parallel arrangement of fibers, better load - carrying capacity was observed in the direction of fiber deposition as compared to the direction perpendicular to fiber deposition. The membrane elements were not shown to carry any load due to out of plane bending. On the other hand , the interconnections (junction points) were idealized as truss elements due to multiple layers of deposition of crossing fibers. The hydrogel was modeled using a solid brick element. Use of Abaqus 6.14 was made to model the idealized versions of the elements of the composite tissue equivalent. The element type allotted to the idealized elements can be found in **Table 4**.

Table 4

Element types and sizes for modeling the tissue equivalent

Idealized elements of the tissue equivalent	**Element type**	**Size of the elements (all units of length are in mm and area in mm^2)**
Membrane	S4	Adjusted according to fiber spacing i.e. 0.8 x 1, 0.4x1 and 0.2 x 1; thickness = 0.016
Truss	T3D2	C/S area = 0.000387; length = 1
Solid brick	C3D8	5 x 5 x 1

The first step to set up the model was initiated by modeling the truss elements followed by membrane elements. The arrangement of truss elements and membrane elements was done in accordance with the spacing of the fibers of the scaffold (**Fig. 20**). The next step was to combine the fiber scaffold and the hydrogel. The embedment feature available in Abaqus allowed to embed the fiber scaffold in the solid hydrogel (**Fig. 21**). Due to this feature, the translational

degrees of freedom of the fiber scaffold (embedded part) were constrained to the degrees of freedom of the hydrogel (host region).

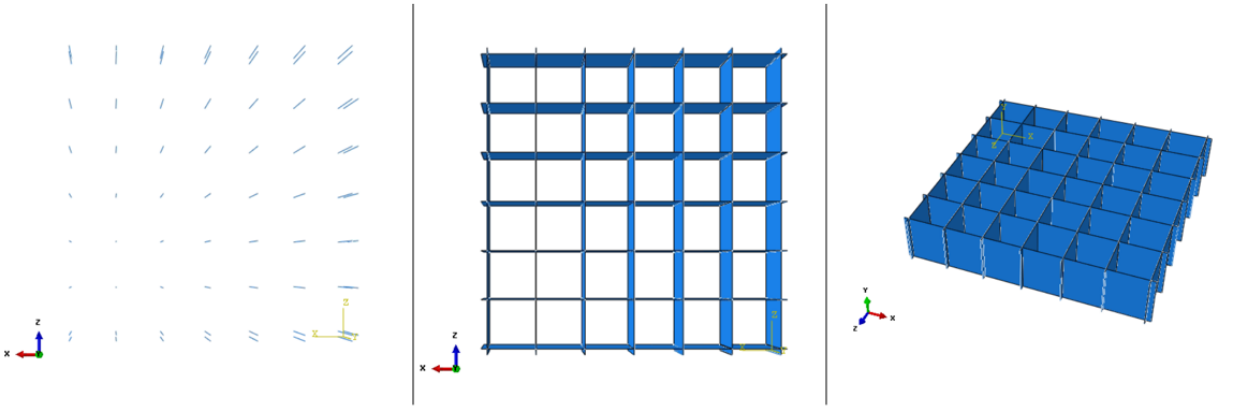

(a)

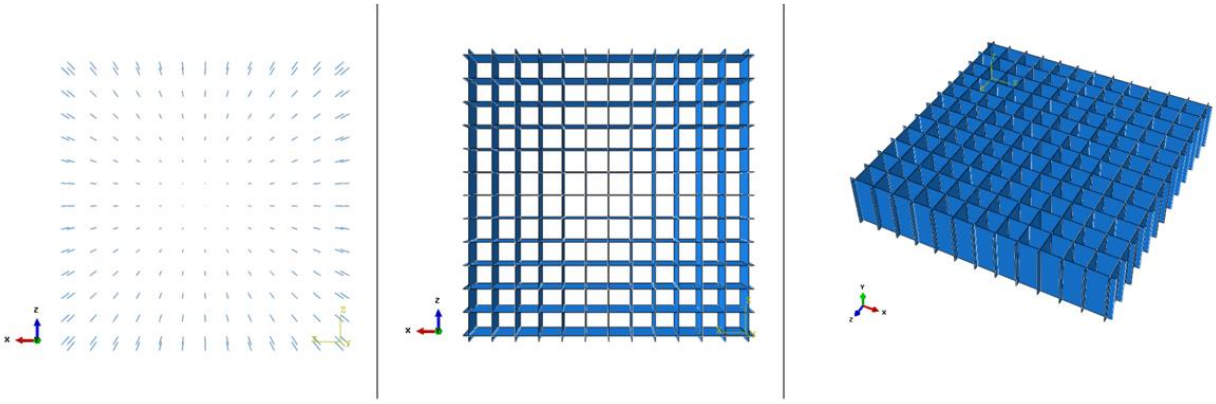

(b)

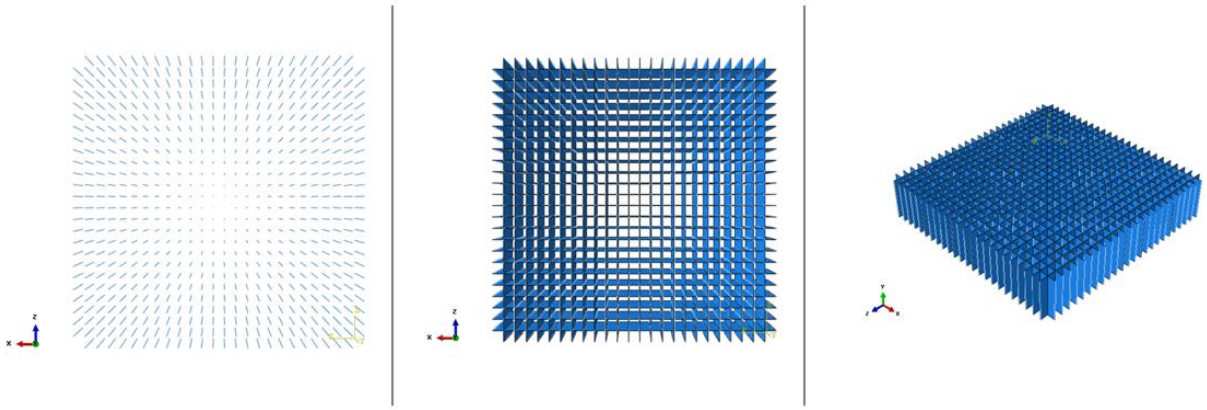

(c)

Fig.20 Arrangement of trusses and membrane and final PCL scaffold (from left to right, with first two figures representing the top view , while the third representing an isometric view) in Abaqus (a) 800 µm spacing scaffold (b) 400 µm spacing scaffold (c) 200 µm spacing scaffold

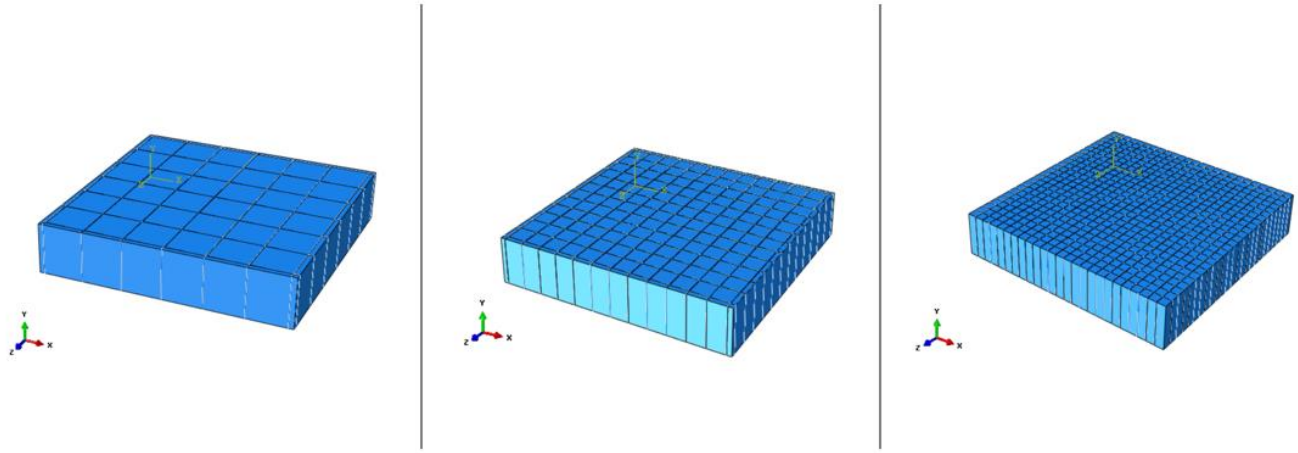

(a) (b) (c)

Fig.21 (a) 800 µm spacing PCL scaffold embedded in gelMA (b) 400 µm spacing PCL scaffold embedded in gelMA (c) 200 µm spacing PCL scaffold embedded in gelMA

2.3.2 Boundary Conditions

To ensure the compatibility between the truss elements and membrane elements, use of tie constraints was made. The truss elements were assigned as the master elements while the membrane elements were assigned as the slave elements. Dirichlet boundary conditions, restraining all the translational degrees of freedom, were assigned on the bottom part of the truss elements (**Fig. 22(a)**). No boundary conditions were provided to the membrane elements in order to avoid the error of over constraining. A reference point on top of the scaffold was provided to which the top surface of the fiber scaffold comprising the nodes of the truss elements were coupled (**Fig. 22(b)**). Displacement of 0.1 was applied through the reference point on the scaffold. The displacement was applied only in the X - direction (**Fig. 22(c)**) while all other degrees of freedom of the reference point were constrained in order to obtain a direct shear loading condition. With these boundary conditions, mechanical response of the scaffold was elicited.

In the case of analyzing the mechanical response of the composite material, as described previously, the scaffold was embedded in the solid hydrogel element. Perfect bonding was assumed between the fiber scaffold and the hydrogel. Similar Dirichlet boundary conditions were applied to the material, only this time to the hydrogel solid element instead of scaffold elements (**Fig. 23**) .

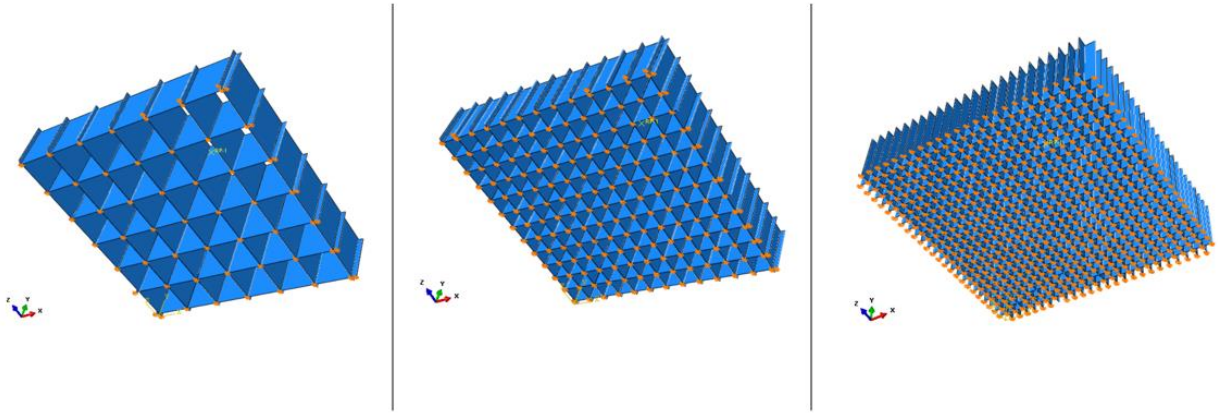

(a)

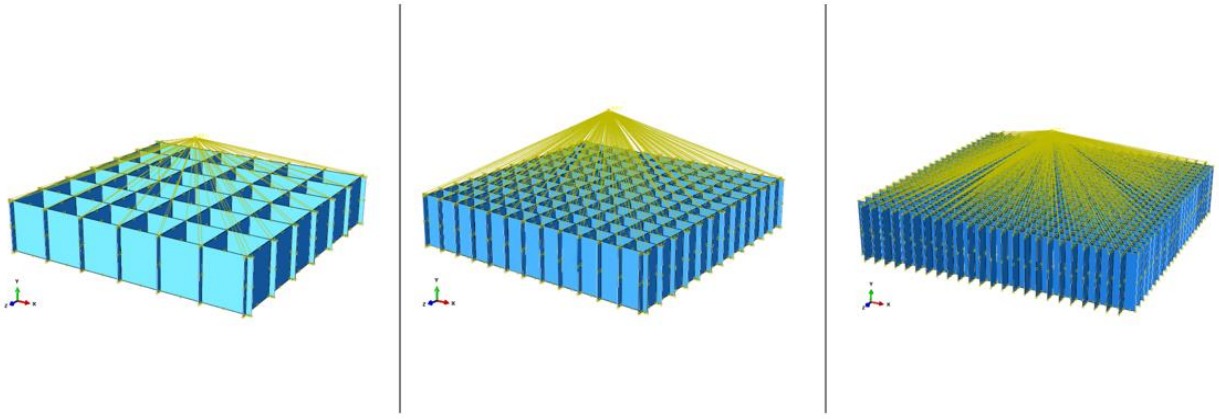

(b)

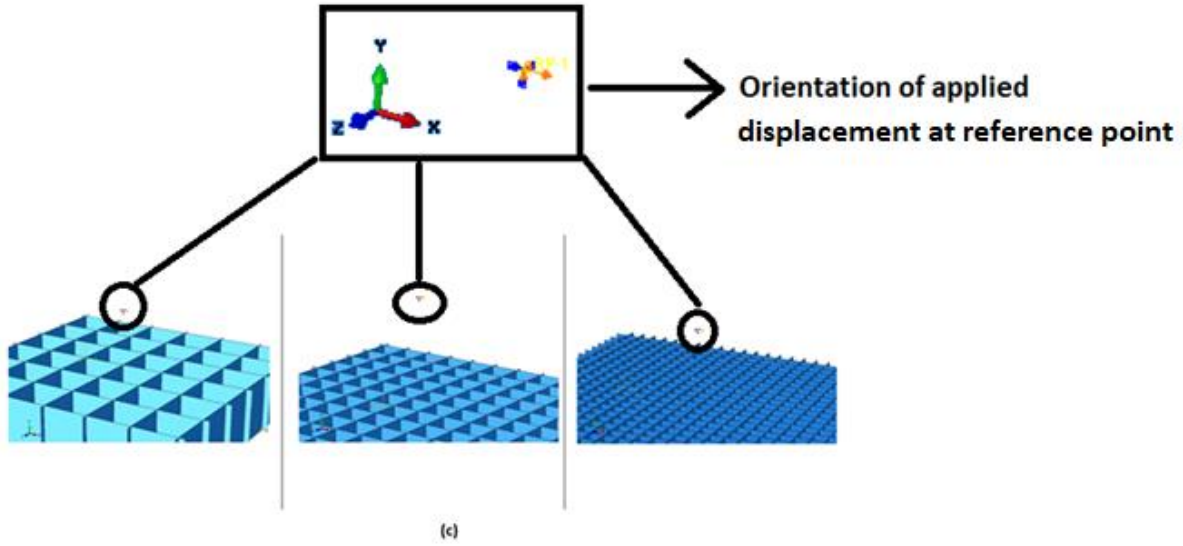

(c)

Fig.22 (a) Dirichlet boundary conditions for PCL scaffolds with 800, 400, 200 μm spacing (from left to right) (b) Coupling condition with reference point (c) Displacement application at reference point

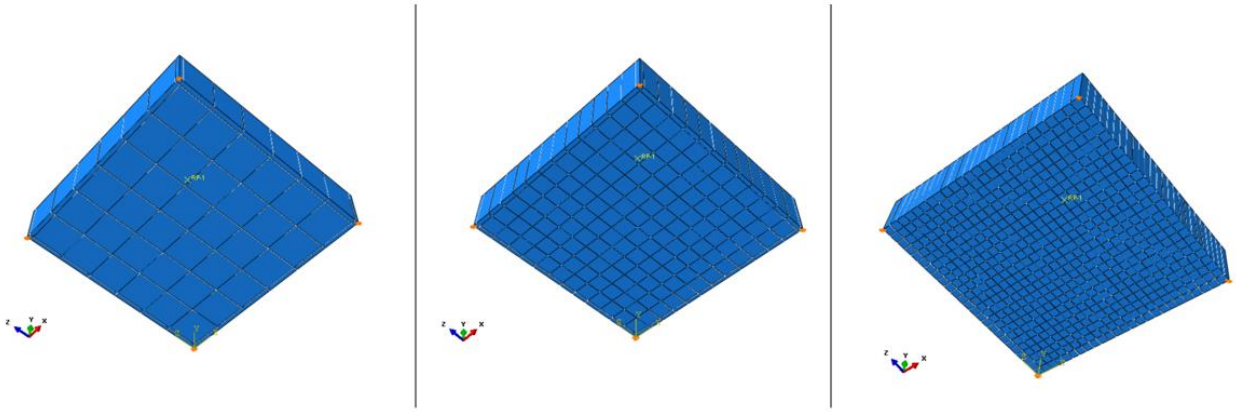

(a)

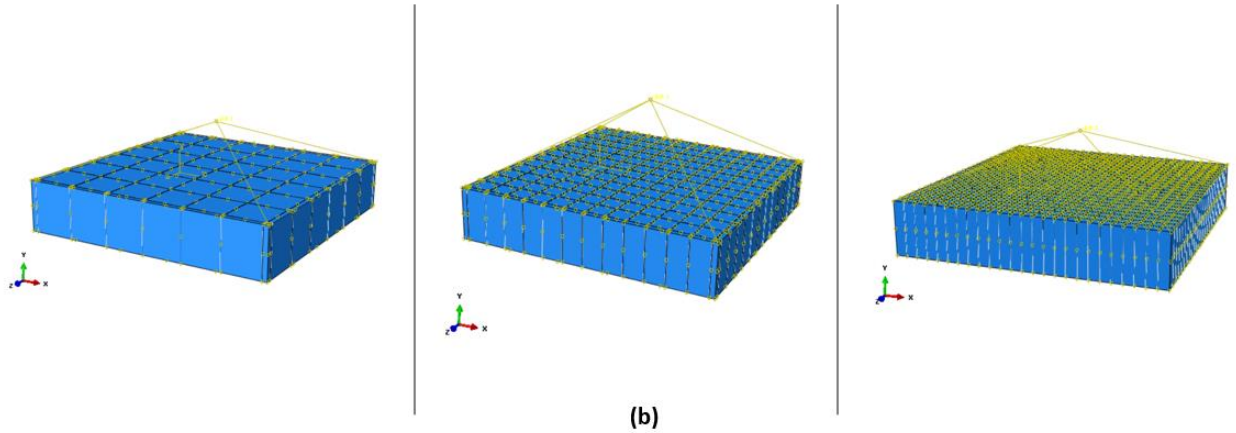

(b)

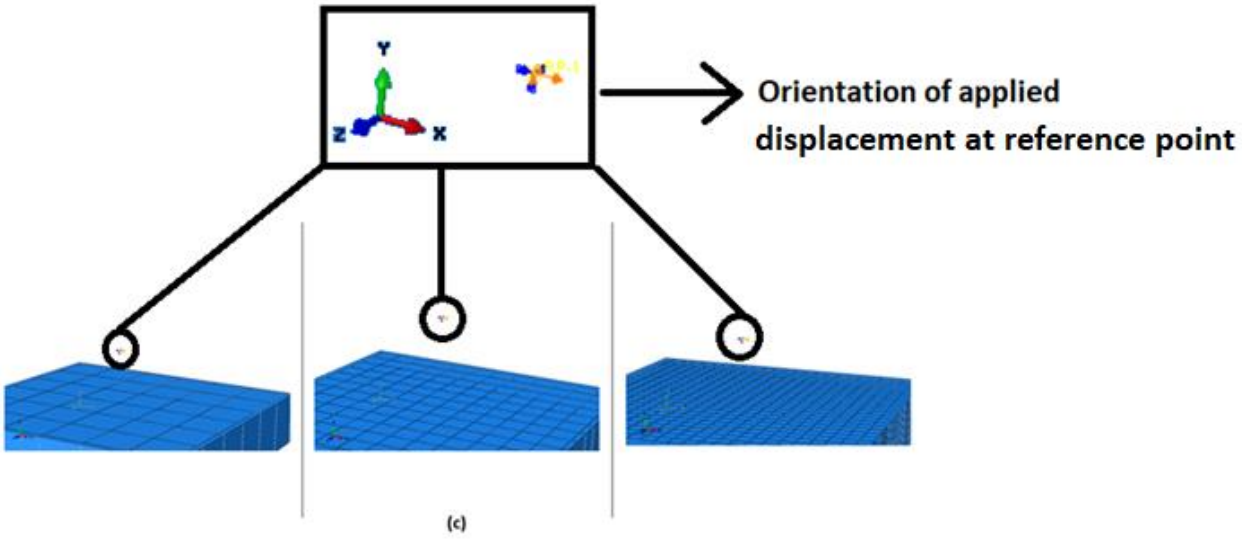

Fig.23 (a) Dirichlet boundary conditions for PCL scaffolds with 800, 400, 200 µm spacing (from left to right) embedded in gelMA (b) Coupling condition with reference point (c) Displacement application at reference point

2.3.3 Validation of the model for mesh size

A validation check was performed in order to determine the mesh size of the model. The mesh refinement was initiated with a global size of 0.1 followed by 0.05 and 0.025 for all the elements. A displacement of 0.1 was initially applied to the scaffold only model at the reference point in order to check the stress distribution in the elements. An irregular stress distribution with highly irregular deformations was observed in the elements as the size of the elements was decreased. This problem was overcome by using only one element for trusses and membranes. For the solid element of hydrogel, the stress distribution in the discretized model was checked with the analytical equation **(ANNEXURE - equation 3),** again by applying a displacement of 0.1 at the reference point **.** Non-uniform stress distribution was observed when the hydrogel element was discretized into 2500 elements (global size of each element - 0.1). However, according to the analytical equation, a uniform stress distribution should be observed in the hydrogel for homogeneous deformation. Uniform stress distribution state was ultimately achieved using 1 element for the hydrogel (**Fig. 24**). Hence, a homogeneous deformation state was obtained using one element (without refinement) for all the components of the model.

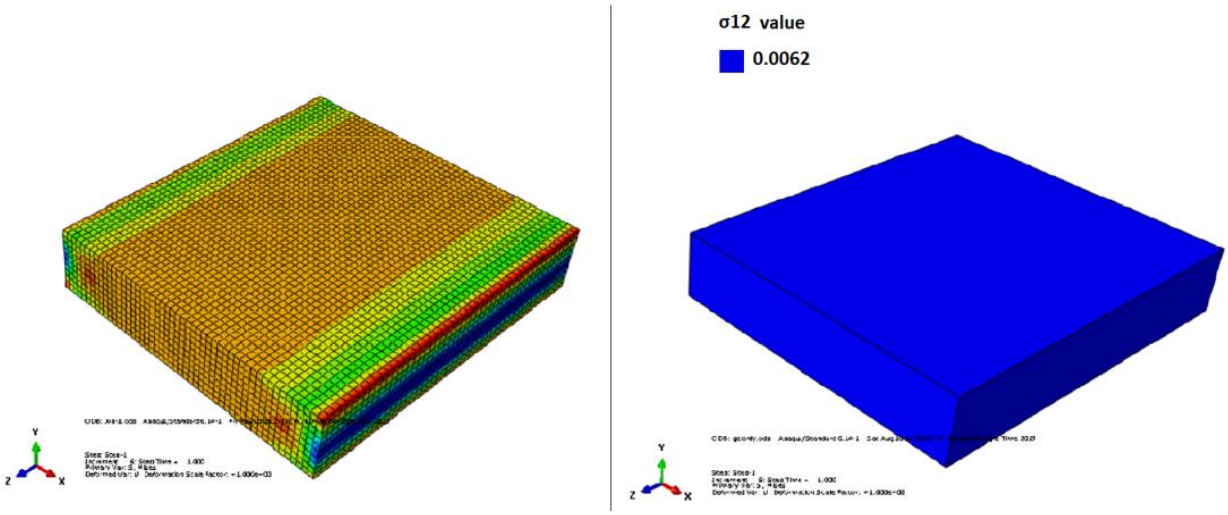

Fig. 24 Validation check for shear stress distribution in hydrogel only **(a)** Non-uniform shear stress distribution observed throughout the hydrogel discretized into 2500 elements **(b)** Uniform shear stress distribution observed in the hydrogel discretized with 1 element

CHAPTER 3

3.1 Results

3.1.1 Fabrication results

Fig.25 shows the electrospun meshes with different fiber spacings. Printing the meshes with 800, 400 and 200 µm spacing with previously mentioned printing parameters resulted in fibers with diameter 16.408 $\pm$ 0.277 µm. Fusion of fibers was observed as they were written with melt-extrusion, giving rise to membrane – like wall structures (**Fig. 26**). Moreover, at the junctions, fused fibers formed column like structures (**Fig. 26**). The result of structural formation of the fiber scaffold was confirmed by comparing it with the study by *Castilho et. al.*[27]. The diameter of these junctions or interconnections was 21.674 $\pm$ 1.452 µm. Effective bonding of gelMA and fiber scaffolds was also confirmed to form the composite constructs (**Fig. 27**)**.**

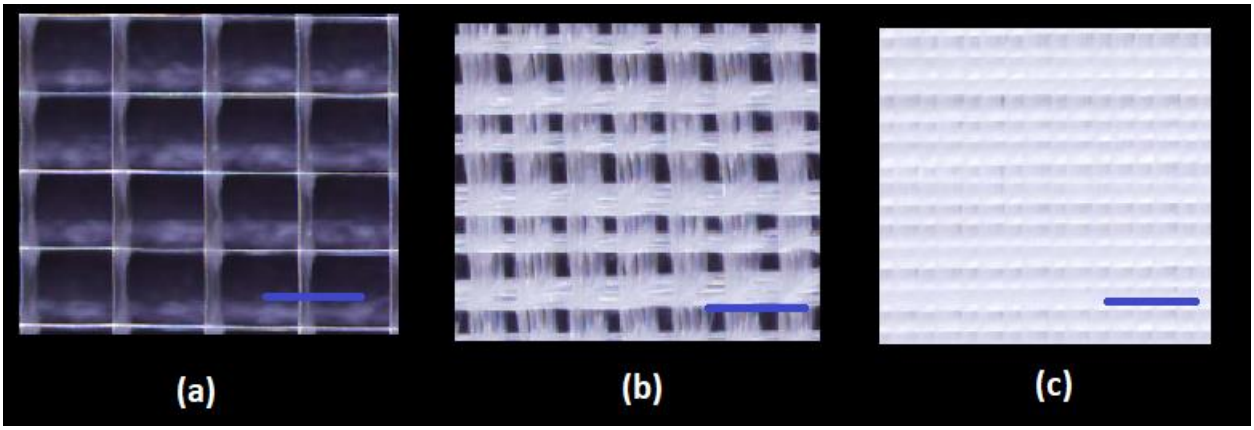

Fig. 25 PCL fiber meshes with three different spacings (a) 800 µm spacing (b) 400 µm spacings (c) 200 µm spacing. *Scale bar = 830 µm*

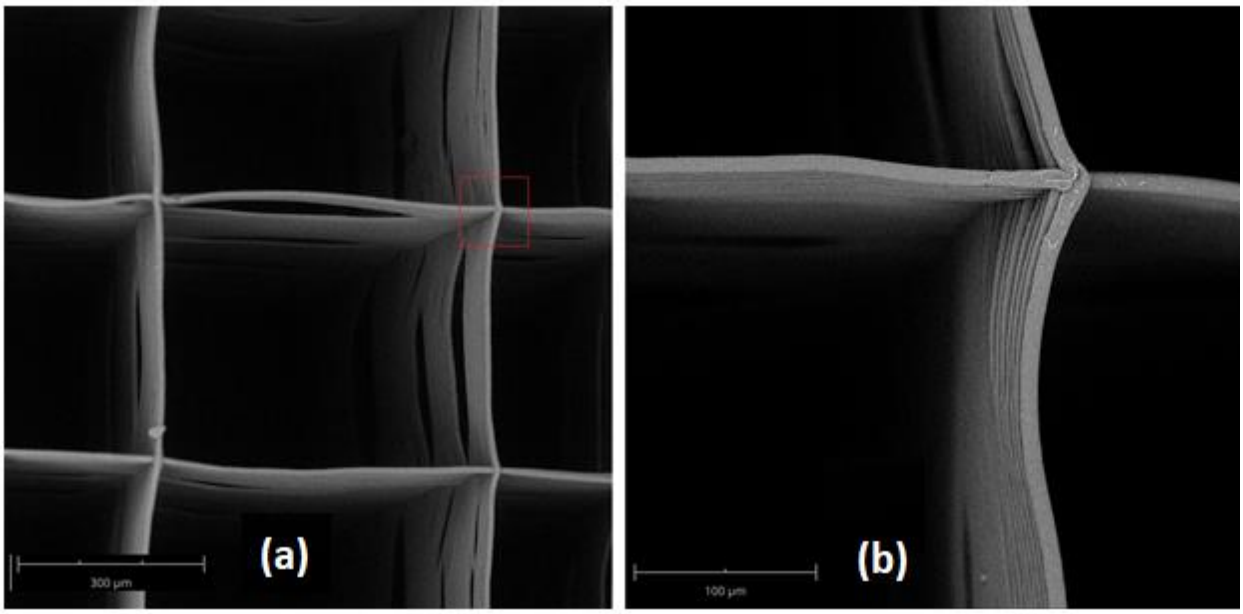

Fig. 26 (a) Scanning electron microscopy image of a MEW printed PCL fiber scaffold. *Scale bar = 300 µm* **(b)** detail of fiber buildup resulting in column like structure at interconnecting point. *Scale bar = 100 µm*

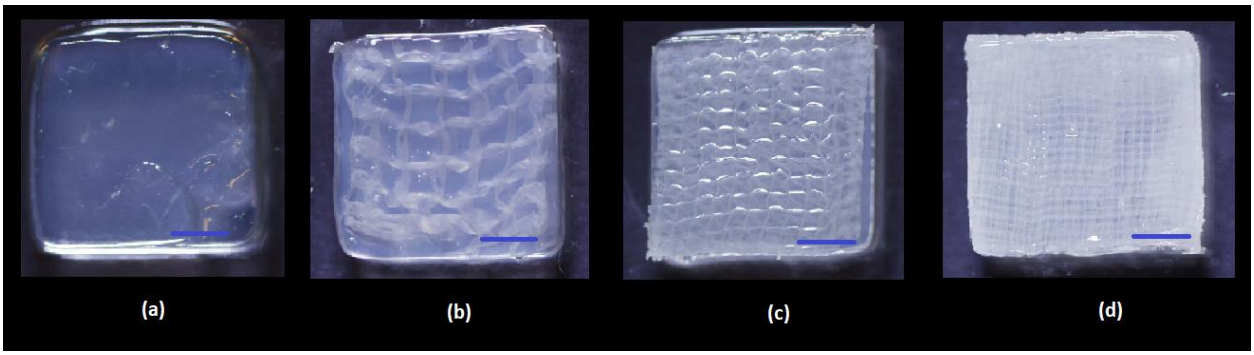

Fig. 27 (a) Hydrogel only (b) 800 µm spacing fiber scaffold embedded in hydrogel (c) 400 µm spacing fiber scaffold embedded in hydrogel (d) 200 µm spacing fiber scaffold embedded in hydrogel. *Scale bar = 300 µm*

3.1.2 Experimental results

For the purpose of characterization, stiffness (K) was attributed to PCL fiber scaffolds and linear elastic shear modulus (G) was attributed to hydrogels. The reason for attributing stiffness to fiber scaffolds was due to the fact that fiber scaffolds do not possess continuity of material throughout the structure. Hence, regions where material is not present will not experience any strain, thereby making stress value at that point invalid. An increase in mean value for stiffness or shear modulus of fiber scaffolds only or composites was observed with decrease in spacing of the fibers of scaffolds. This trend can be clearly observed in the plots of force vs. displacement for scaffolds

only and stress vs. strain for hydrogels **(Fig. 28 and 29)**. The statistical tests on the experimental results of fiber scaffolds only yielded no significant difference in mean stiffness values for $\alpha = 0.05$. On the other hand, the statistical tests for hydrogel and composites yielded a significant difference in mean shear moduli with $p < 0.05$.

The value for shear modulus for gelMA only hydrogel was further used in the computational analysis of the model to define the material parameters for the solid element.

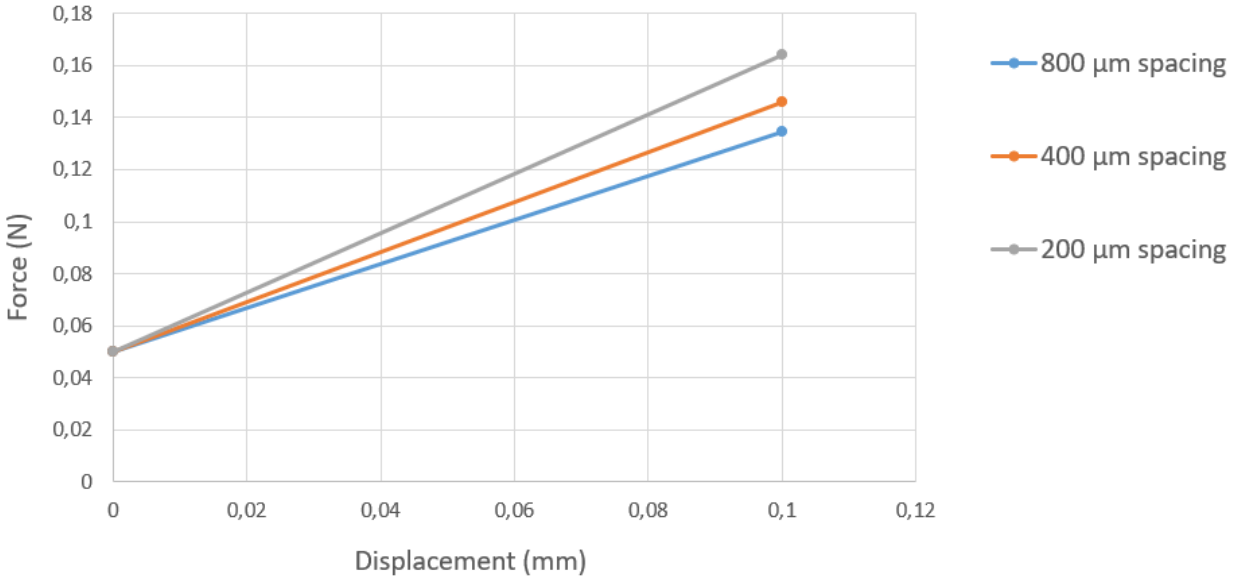

(a)

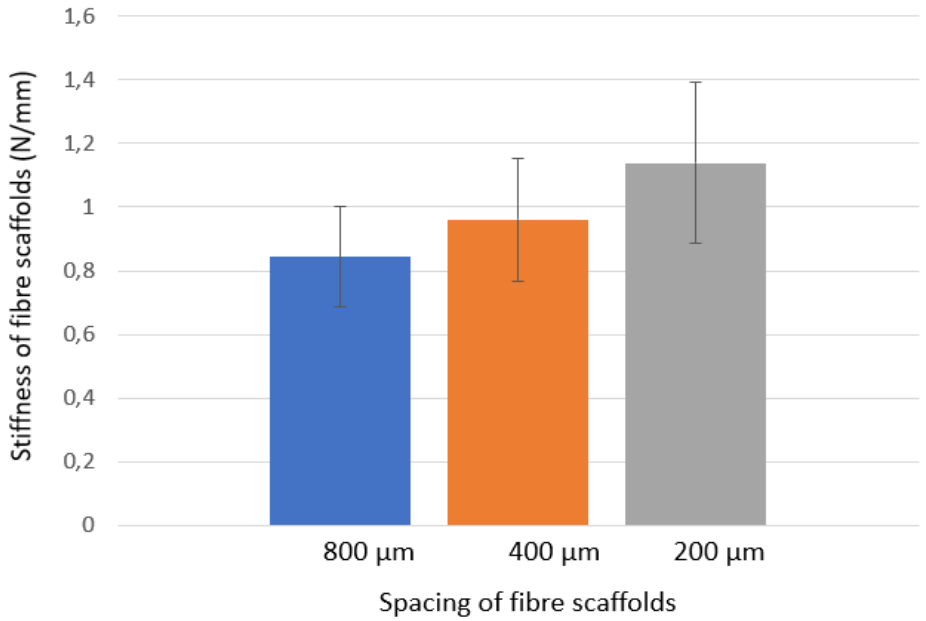

(b)

Fig. 28 (a) Force vs. displacement curves for PCL fiber scaffolds (b) Representation of variation of stiffness of PCL fiber scaffolds with respect to fiber spacing. Data represented as mean ± std. error.

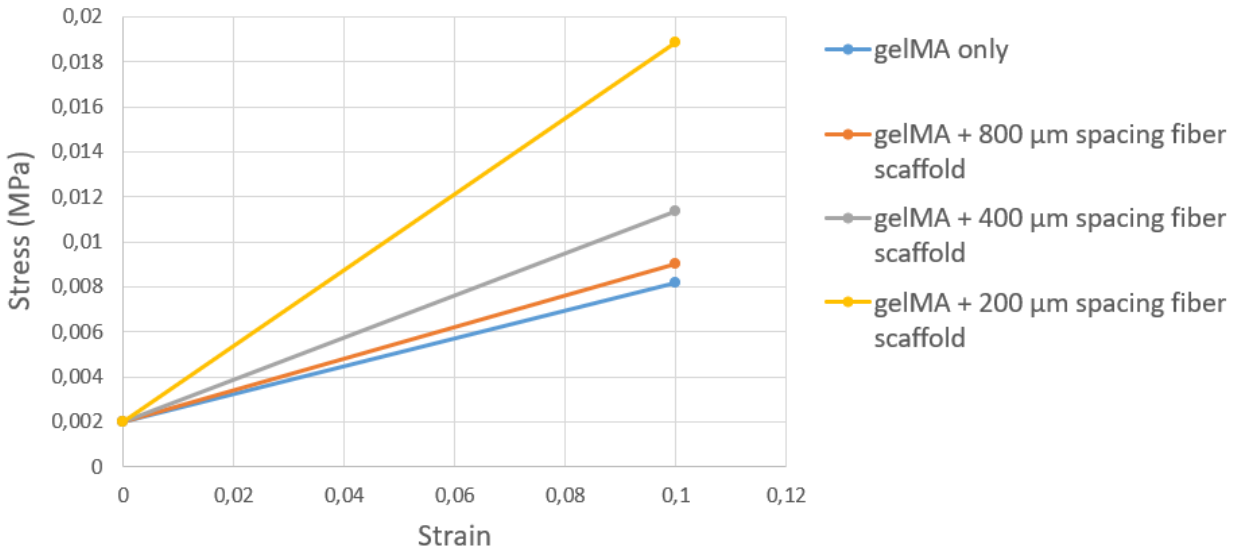

(a)

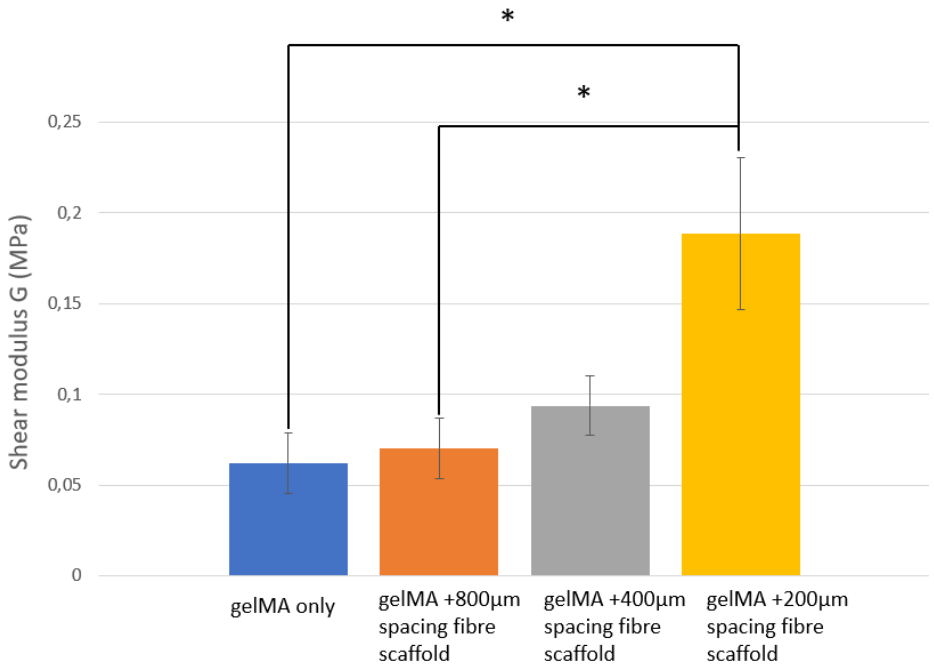

(b)

Fig. 29 (a) Stress vs. strain curves for hydrogel and composites (b) Representation of variation of shear moduli hydrogel and composites. Data represented as mean ± std error, * = p< 0.05.

3.1.3 Computational results

The shear modulus of gelMA was the main component to be determined as the study is concerned with shear properties of the tissue equivalent. However, other material parameters were adopted from the previous study by *Castilho et. al.*[27] **(Table 5)**. It has to be noted that even though the value of Young's modulus was considered as 3 MPa for interconnections, the value considered in this study is 182 MPa. This is because under shear deformation, the a material invariably experience tensile stresses along the diagonal **(Fig. 3)**. Since it was assumed from the mechanical response of a material undergoing shear deformation that PCL scaffold interconnections would rotate and align in the direction of tensile stress region along the diagonal, a Young's modulus of 182 MPa, which is the Young's modulus for PCL fibers under tensile loading [27], was assigned to interconnection elements.

It is to be noted that even though gelMA material in the previous study was considered to be a compressible Neo-Hookean material, from mathematical deductions **(ANNEXURE),** it can be concluded that there is a linear correlation between shear stress and shear deformation (or strain) for shear deformation $\gamma \rightarrow 0$. Hence, to simplify the analysis, a Neo-Hookean material was

converted to a linear elastic material. The value of Young's modulus was found by simply applying the equation:

$E = 2G(1+\nu)$ (where ν is 0.49 [27]).

Table 5

Material type and parameters for different components of FEM model

Component of tissue equivalent FEM model	Material type	Material parameters
Interconnection	Isotropic Linear elastic	E = 182 MPa ; ν = 0.3
Membrane	Orthotropic linear elastic	E_1 = 182 MPa; E_2 = 0.06 MPa; ν_{12} = 0.43; G_{12} = 0.88; G_{13} = 1E10^{-7} MPa; G_{23} = 1E10^{-7} MPa
Hydrogel - gelMA	Neo-Hookean compressible material converted to isotropic linear elastic	E = 0.185 MPa; ν = 0.49

After incorporating these values in the computational models defined in Chapter 2, the stiffness of PCL fiber scaffolds and shear modulus of fiber scaffold embedded hydrogels were found out **(Tables 6 and 7)** by performing a linear elastic analysis. The reaction force obtained at the reference point defined in the model was plotted against the displacement in order to determine the stiffness. In the case of hydrogels, the force at the reference point was divided by the top surface of the hydrogel (5 x 5 mm) to derive the shear stress value. The strain value would be equal to the value of the displacement applied to the sample as the thickness of the sample is 1 mm. Hence, shear modulus for the hydrogels was derived by simply taking a slope of stress vs. strain curve. Comparative graphs of the experimental results and the computational results were then plotted **(Fig. 30 and 31)**.

Table 6

Stiffness of PCL fiber scaffolds for different fiber spacings

Fiber spacing	Stiffness K (N/mm)
800 µm	0.493
400 µm	0.915
200 µm	1.690

Table 7

Shear moduli for composite hydrogels

Composite hydrogels	Shear Modulus G (MPa)
gelMA + 800 µm spacing PCL scaffold	0.0866
gelMA + 400 µm spacing PCL scaffold	0.107
gelMA + 200 µm spacing PCL scaffold	0.146

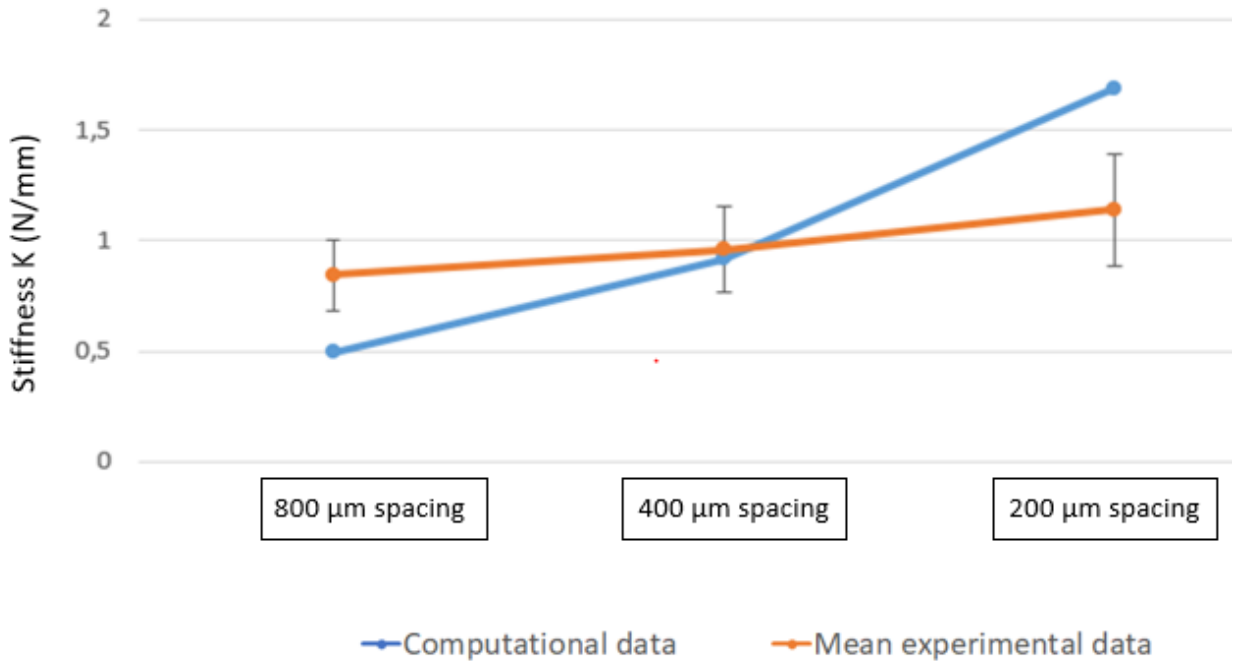

Fig. 30 Comparative representation of shear moduli for computational data and mean experimental data for PCL fiber scaffolds

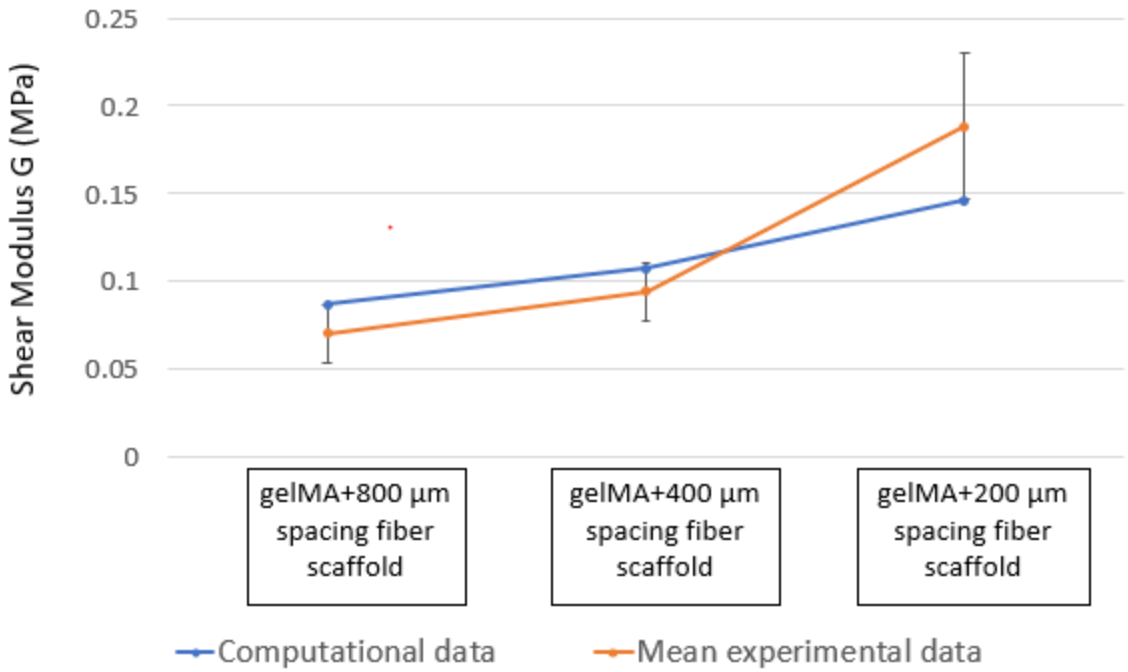

Fig. 31 Comparative representation of shear moduli for computational data and mean experimental data for gelMA + fiber scaffolds

CHAPTER 4

4.1 Discussion

The final implication of this study would be to elicit the behavior of the composite tissue equivalent comparable to the articular cartilage. As it can be observed from studies for compressive loading that a higher Young's modulus is exhibited with higher volume fraction of fibers in hydrogel [26,27,29], similar behavior can be expected with respect to shear modulus. As expected, an increase in shear modulus is observed in hydrogels embedded with scaffolds with lower inter-fiber spacing. Correspondingly, an increase in stiffness was observed with a decrease in fiber spacing for scaffold only samples. It is to be noted that a displacement value of 0.1 was directly applied to the computational model since our interest lay in obtaining the value of either the stiffness or the shear modulus corresponding to physiological strain value , i.e. 0.1 [30]. Replicating the experimental force application for the computational model would invariably result in the same value of stiffness since the analysis is taking place in linear elastic regime. Hence, for ease of analysis and post processing results, 0.1 mm displacement was directly applied in the computational model.

This trend of increasing resistance to shear deformation is owing to the structural response of the box - structured scaffolds. The truss elements and membrane elements give a structural response similar to that of framed structures with trusses acting as columns and membranes as connecting elements for the trusses. Under the action of shear displacement in X-direction **(Fig. 32)**, the trusses or the interconnection elements act as rigid elements as compared to the membrane elements owing to their large diameters and high Young's modulus. This creates a rigid body rotation of the truss elements, therefore producing no stress in those elements **(Fig.33)**. However, the rotation under a horizontal displacement (shear deformation) of the entire structure (scaffold) is resisted by the membrane elements. Since the truss elements produce a rigid body rotation at a given point under the action of horizontal displacement applied at the top of the elements, the instability of the entire structure is avoided by the tying action of the membrane elements. This kind of tying action produces shear stress in the membrane elements. The membranes perpendicular to the direction of shear deformation do not participate in resisting shear deformation **(Fig. 34)**. This explanation renders the understanding that better shear load resisting capacity can be introduced by increasing the number of membranes. The decrease in fiber spacing will, by default, increase the membrane elements and hence the trend of increasing stiffness with decrease in fiber spacing has been found true.

Despite a good agreement between the computational model and the mean experimental data for PCL fiber scaffold with 400 µm spacing (with and without embedding in hydrogel), the computational value of stiffness for 800 µm spacing PCL fiber scaffold is 0.6 times that of mean experimental value, while the computational result of shear modulus for gelMA + 800 µm spacing PCL fiber scaffold is 1.24 times that of mean experimental value. Similar is the case for 200 µm spacing PCL fiber scaffold, where the computational result of stiffness is 1.48 times the mean

experimental value and that of computational shear modulus value for gelMA + for 200 µm spacing PCL fiber scaffold is almost 0.78 times the value of mean experimental value **(Fig. 30 and 31)**.

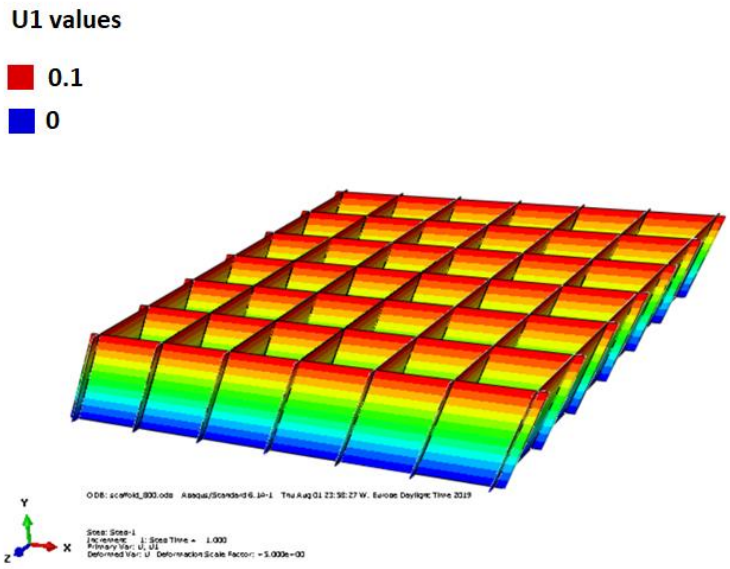

Fig. 32 Displacement profile in U1 (X-direction) of the scaffold

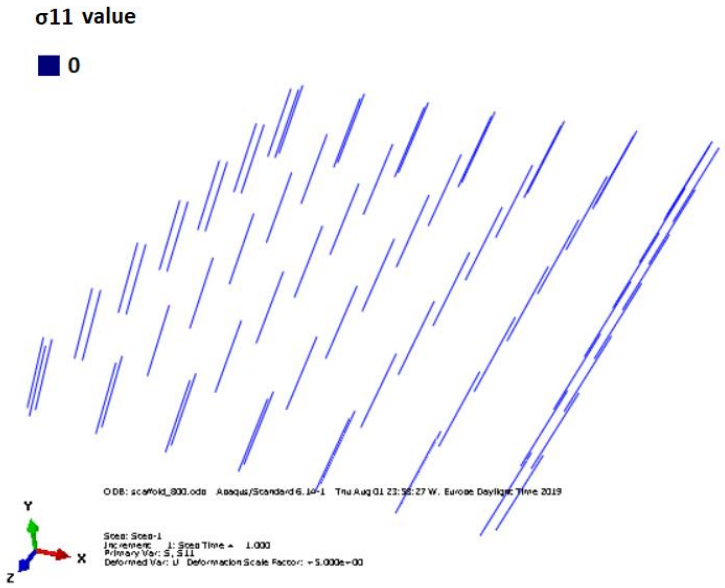

Fig. 33 Normal stresses in truss elements

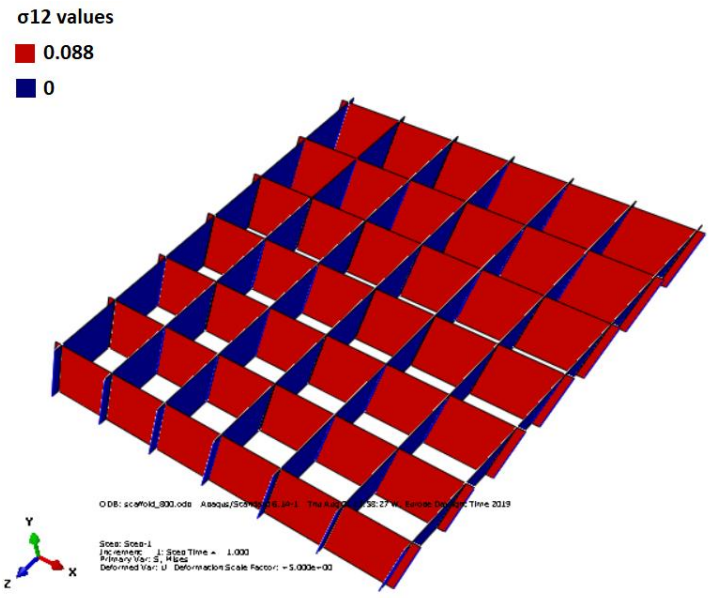

Fig. 34 Shear stress distribution in membrane elements

Moreover, there are certain parameters which need to be taken care of in order to test the tissue equivalents and fiber scaffolds in order to understand the true behavior of the material.

Beginning with the experimental setup, a shear clamp designed specifically to perform pure shear testing can be used instead of modifying a tension film clamp to perform the shear tests. Even though care was to taken to sustain the accuracy of testing, utilizing a setup meant for different type of loading condition leaves room for errors. The shear plates used for testing were made from the resin R05 using DLP 3D printing. A stiffer material from the category of metals could be utilized in order to avoid errors in design, such as minor bending of shear plates due to DLP 3D printing. To provide the boundary conditions to samples, use of cyanoacrylate (ergo.® 5400 kunststoff) was made. It was observed that cyanoacrylate altered the material properties at the point of contact. It was also difficult to control the amount of superglue applied on the shear plate as there was no fixed estimated quantity that could be applied. Any increase or decrease in the amount of superglue hampered with the boundary conditions of the sample.

The use of superglue would also in general affect the boundary conditions in the computational model. As seen before, the Dirichlet boundary conditions used for the scaffold and hydrogel were simply restricting translation in the U1, U2 and U3 (X, Y and Z) directions, fixing the sample on a shear plate would also constrain the rotation at the point that point. Since truss and membrane elements were used in the model which had only linear degrees of freedom, constraining rotation at the ends where boundary conditions were provided would rather prove redundant. Similar is the case when it comes to providing boundary conditions for the hydrogels. However, the

rotation generating moment would be extremely less due to the low value of thickness of the sample (1 mm in our case) and therefore, it was ignored for FEM analysis in this study. But for a more realistic model, a boundary condition which restricts rotation should exist.

Lastly , even though 182 MPa was considered as the Young's modulus value for the interconnections, it was observed that the fusion of the fibers was not completely achieved at the overlapping regions of the fibers. This leaves scope for further testing the tensile property of the interconnections. This can be done by performing a tensile test on an individual interconnection by separating it from the rest of the scaffold.

Future scope for research would entail characterization of the tissue equivalent by infusing it with cells and studying the effects of extracellular matrix (ECM) build up in the material as well as adopting complex material models such as viscoelasticity. Meticulous computational modeling approaches will have to be generated in order to capture complex material responses which will further eliminate the need for experimental testing for different geometries of the fiber scaffolds embedded in hydrogel. The study also leaves an open question with respect to analyzing the combined loading condition, i.e. shear and compression, which are the two predominant forces on an articular cartilage, on the tissue equivalent.

CHAPTER 5

5.1 Conclusion

The present study posits results of the reinforcement effect of PCL fiber scaffolds in hydrogels under shear deformation. The reinforcement of hydrogel with fiber scaffolds certainly increases the shear modulus as compared to hydrogel only. Maximum reinforcing effect leading to the highest shear modulus of the composites from the given samples is evident in fiber scaffold with 200 µm spacing. An association with decreasing fiber spacing and increasing shear modulus of composites has thus been drawn. The deformable membrane elements have been shown to dominate the reinforcement mechanism in the hydrogel. The computational models have aptly showcased the increasing trend in the shear modulus of the composites with the decrease in fiber spacing. Hence, use of computational modeling can be considered as an appropriate method for determining the stiffness of such tissue equivalents. Thus, the results of the present study provide new fundamental insights into the shear deformation of gelMA and PCL fiber based tissue equivalents.

Acknowledgements

I would like to express my sincere gratitude to my supervisor Ms. Mylene de Ruijter for providing me her invaluable guidance and motivation throughout the course of the project. I would also like to be thankful to Dr. Miguel Castilho and Dr. Mohammad Mirzaali for their technical guidance and inputs pertaining to computational modeling. Also, I would like to thank Dr. Jie Zhou for all the comments and suggestions that helped me complete my project successfully.

ANNEXURE

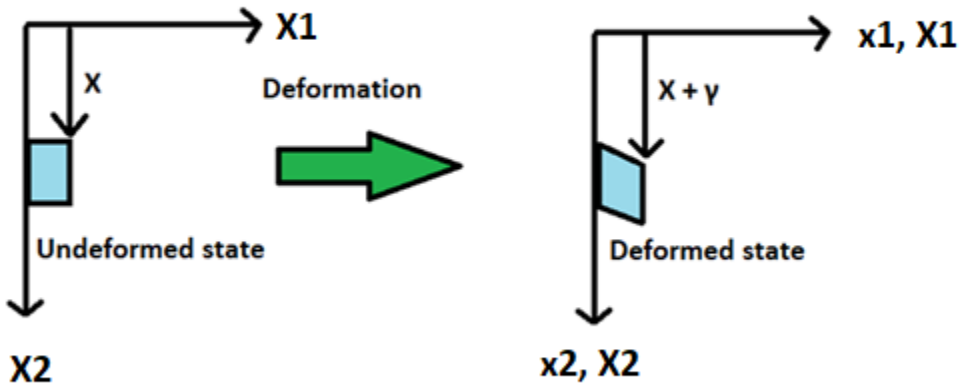

Fig. 35 Schematic representation of deformation mapping of the sample experiencing homogeneous shear deformation

Deformation field applied to sample ***(Fig. 35)****:*

$x1 = X1 + \gamma\, X2\ ;\ x2 = X2\ ;\ x3 = X3$

Where (X1, X2 , X3) are the coordinates of the sample in reference configuration and (x1, x2, x3) are the coordinates of the sample in the deformed configuration.

$$\Rightarrow \textit{Deformation gradient } (F) = \begin{bmatrix} \frac{\partial x1}{\partial X1} & \frac{\partial x1}{\partial X2} & \frac{\partial x1}{\partial X} \\ \frac{\partial x2}{\partial X1} & \frac{\partial x2}{\partial X2} & \frac{\partial x2}{\partial X3} \\ \frac{\partial x3}{\partial X1} & \frac{\partial x3}{\partial X2} & \frac{\partial x3}{\partial X3} \end{bmatrix}$$

$$\therefore F = \begin{bmatrix} 1 & \gamma & 0 \\ 0 & 1 & 0 \\ 0 & 0 & 1 \end{bmatrix} \qquad (1)$$

$\Rightarrow$ *Cauchy-Green Tensor (B) = F*F^T*

$$\therefore B = \begin{bmatrix} 1+\gamma 2 & \gamma & 0 \\ \gamma & 1 & 0 \\ 0 & 0 & 1 \end{bmatrix} \qquad (2)$$

GelMA was considered as a compressible Neo-Hookean hyperleastic material.

Therefore, the strain energy density (SED) function W (I_1, J) = $\frac{\mu}{2} * (\overline{I_1} - 3) + \frac{1}{D1} * (J-1)^2$

where $\overline{I_1} = J^{-2/3} * I_1$; $I_1 = \lambda_1^2 + \lambda_2^2 + \lambda_3^2$ *and J = det(F) (* λ_1, λ_2 *and* λ_3 *are the principal stretches).*

$\Rightarrow$ *Cauchy stress (*σ*) =* $\frac{2}{J} F \frac{\partial W}{\partial C} F^T = \frac{2}{J} \frac{\partial W}{\partial I_1} B + \frac{\partial W}{\partial J} I$

(where C = $F^T * F$ *and I is the second order identity tensor)*

$$\therefore \sigma = \left[\frac{2}{J} * \frac{\mu}{2} * J^{-\frac{2}{3}} * \left(\frac{\partial I_1}{\partial I_1} - 0\right) + 0\right] * B + \left[\left(\frac{\mu}{2} * -\frac{2}{3} * J^{\frac{-5}{3}} * I_1\right) + \left(\frac{1}{D_1} * 2 * (J-1)\right)\right] * I$$

$$\therefore \sigma = \left[\frac{2}{1} * \frac{\mu}{2} * 1 * (I - 0)\right] * B + \left[\left(\frac{\mu}{2} * -\frac{2}{3} * 1 * I_1\right) + 0\right] * I$$

($On\ applying\ J = 1$ *and the constraint* $I_1 - 3J^{\frac{2}{3}} = 0$ *) [42]*

$$\therefore \sigma = \mu * B - \mu * I$$

$$\therefore \sigma = \mu * (B - I)$$

(Substituting values of B and I)

$$\therefore \begin{bmatrix} \sigma_{11} & \sigma_{12} & \sigma_{13} \\ \sigma_{21} & \sigma_{22} & \sigma_{23} \\ \sigma_{31} & \sigma_{32} & \sigma_{33} \end{bmatrix} = \mu * \begin{bmatrix} \gamma^2 & \gamma & 0 \\ \gamma & 0 & 0 \\ 0 & 0 & 0 \end{bmatrix} \qquad (3)$$

This means that for values of $\gamma \to 0$, the effect of γ^2 diminishes. Therefore, a state of pure shear can be achieved without any additional boundary condition to be provided for σ_{11}.

A direct relationship of shear stress and shear deformation can be achieved from this equation , i.e. $\sigma_{12} = \mu * \gamma$.

References

[1] DeWitt, N., 2008. Regenerative medicine. *Nature*, *453*(7193), p.301.

[2] Van Osch, G.J., Brittberg, M., Dennis, J.E., Bastiaansen-Jenniskens, Y.M., Erben, R.G., Konttinen, Y.T. and Luyten, F.P., 2009. Cartilage repair: past and future–lessons for regenerative medicine. *Journal of Cellular and Molecular Medicine*, *13*(5), pp.792-810.

[3] Mandelbaum, B.R., Browne, J.E., Fu, F., Micheli, L., Mosely, J.B., Erggelet, C., Minas, T. and Peterson, L., 1998. Articular cartilage lesions of the knee. *The American Journal of Sports Medicine*, *26*(6), pp.853-861.

[4] Bijlsma, J.W., Berenbaum, F. and Lafeber, F.P., 2011. Osteoarthritis: an update with relevance for clinical practice. *The Lancet*, *377*(9783), pp.2115-2126.

[5] Klein, T.J., Rizzi, S.C., Reichert, J.C., Georgi, N., Malda, J., Schuurman, W., Crawford, R.W. and Hutmacher, D.W., 2009. Strategies for zonal cartilage repair using hydrogels. *Macromolecular Bioscience*, *9*(11), pp.1049-1058.

[6] Vacanti, J.P. and Langer, R., 1999. Tissue engineering: the design and fabrication of living replacement devices for surgical reconstruction and transplantation. The Lancet, 354, pp.S32-S34.

[7] Saul, J.M. and Williams, D.F., 2011. Hydrogels in regenerative medicine. In Handbook of Polymer Applications in Medicine and Medical Devices (pp. 279-302). William Andrew Publishing.

[8] Croisier, F., Duwez, A.S., Jérôme, C., Léonard, A.F., Van Der Werf, K.O., Dijkstra, P.J. and Bennink, M.L., 2012. Mechanical testing of electrospun PCL fibers. *Acta Biomaterialia*, *8*(1), pp.218-224.

[9] Shepherd, D.E.T. and Seedhom, B.B., 1999. Thickness of human articular cartilage in joints of the lower limb. *Annals of the Rheumatic Diseases*, *58*(1), pp.27-34.

[10] Cowin, S.C. and Doty, S.B., 2007. *Tissue mechanics*. Springer Science & Business Media.

[11] Shepherd, D.E.T. and Seedhom, B.B., 1999. Thickness of human articular cartilage in joints of the lower limb. *Annals of the rheumatic diseases*, *58*(1), pp.27-34.

[12] Klika, V., Gaffney, E.A., Chen, Y.C. and Brown, C.P., 2016. An overview of multiphase cartilage mechanical modelling and its role in understanding function and pathology. Journal of the Mechanical Behavior of Biomedical Materials, 62, pp.139-157.

[13] Schinagl, R.M., Gurskis, D., Chen, A.C. and Sah, R.L., 1997. Depth-dependent confined compression modulus of full-thickness bovine articular cartilage. *Journal of Orthopaedic Research*, *15*(4), pp.499-506.

[14] Cohen, N.P., Foster, R.J. and Mow, V.C., 1998. Composition and dynamics of articular cartilage: structure, function, and maintaining healthy state. *Journal of Orthopaedic & Sports Physical Therapy*, *28*(4), pp.203-215.

[15] Zhang, X., Blalock, D. and Wang, J., 2015. Classifications and definitions of normal joints. In *Osteoarthritis-progress in Basic Research and Treatment*. IntechOpen.

[16] Tomatsu, T.A.I.S.U.K.E., Imai, N.O.Z.O.M.U., Takeuchi, N.O.R.I.O., Takahashi, K. and Kimura, N., 1992. Experimentally produced fractures of articular cartilage and bone. The effects of shear forces on the pig knee. *The Journal of Bone and Joint Surgery. British volume*, *74*(3), pp.457-462.

[17] Wong, B.L., Bae, W.C., Chun, J., Gratz, K.R., Lotz, M. and Sah, R.L., 2008. Biomechanics of cartilage articulation: effects of lubrication and degeneration on shear deformation. *Arthritis & Rheumatism: Official Journal of the American College of Rheumatology*, *58*(7), pp.2065-2074.

[18] Van Rossom, S., Smith, C.R., Thelen, D.G., Vanwanseele, B., Van Assche, D. and Jonkers, I., 2018. Knee joint loading in healthy adults during functional exercises: implications for rehabilitation guidelines. *Journal of Orthopaedic & Sports Physical Therapy*, *48*(3), pp.162-173.

[19] Visser, J., 2015. *Biofabrication of implants for articular joint repair: Cartilage Regeneration in Reinforced Gelatin-Based Hydrogels* (Doctoral dissertation, Utrecht University).

[20] Mow, V.C., Holmes, M.H. and Lai, W.M., 1984. Fluid transport and mechanical properties of articular cartilage: a review. *Journal of Biomechanics*, *17*(5), pp.377-394.

[21] Hayes, W.C. and Bodine, A.J., 1978. Flow-independent viscoelastic properties of articular cartilage matrix. *Journal of Biomechanics*, *11*(8-9), pp.407-419.

[22] Setton, L.A., Elliott, D.M. and Mow, V.C., 1999. Altered mechanics of cartilage with osteoarthritis: human osteoarthritis and an experimental model of joint degeneration. *Osteoarthritis and Cartilage*, *7*(1), pp.2-14.

[23] Spirt, A.A., Mak, A.F. and Wassell, R.P., 1989. Nonlinear viscoelastic properties of articular cartilage in shear. *Journal of Orthopaedic Research*, *7*(1), pp.43-49.

[24] Wilson, W., Van Donkelaar, C.C., Van Rietbergen, R. and Huiskes, R., 2005. The role of computational models in the search for the mechanical behavior and damage mechanisms of articular cartilage. *Medical Engineering & Physics*, *27*(10), pp.810-826.

[25] Hayes, W.C. and Mockros, L.F., 1971. Viscoelastic properties of human articular cartilage. *Journal of Applied Physiology*, *31*(4), pp.562-568.

[26] Visser, J., Melchels, F.P., Jeon, J.E., Van Bussel, E.M., Kimpton, L.S., Byrne, H.M., Dhert, W.J., Dalton, P.D., Hutmacher, D.W. and Malda, J., 2015. Reinforcement of hydrogels using three-dimensionally printed microfibres. *Nature Communications*, *6*, p.6933.

[27] Castilho, M., Hochleitner, G., Wilson, W., Rietbergen, B., Dalton, P.D., Groll, J., Malda, J. and Ito, K., 2018. Mechanical behavior of a soft hydrogel reinforced with three-dimensional printed microfibre scaffolds. *Scientific Reports*, *8*(1), p.1245.

[28] Bas, O., Lucarotti, S., Angella, D.D., Castro, N.J., Meinert, C., Wunner, F.M., Rank, E., Vozzi, G., Klein, T.J., Catelas, I. and De-Juan-Pardo, E.M., 2018. Rational design and fabrication of multiphasic soft network composites for tissue engineering articular cartilage: A numerical model-based approach. *Chemical Engineering Journal*, *340*, pp.15-23.

[29] Bas, O., De-Juan-Pardo, E.M., Meinert, C., D'Angella, D., Baldwin, J.G., Bray, L.J., Wellard, R.M., Kollmannsberger, S., Rank, E., Werner, C. and Klein, T.J., 2017. Biofabricated soft network composites for cartilage tissue engineering. *Biofabrication*, *9*(2), p.025014.

[30] de Ruijter, M., Hrynevich, A., Haigh, J.N., Hochleitner, G., Castilho, M., Groll, J., Malda, J. and Dalton, P.D., 2018. Out-of-Plane 3D-Printed Microfibers Improve the Shear Properties of Hydrogel Composites. *Small*, *14*(8), p.1702773.

[31] Zhu, W., Mow, V.C., Koob, T.J. and Eyre, D.R., 1993. Viscoelastic shear properties of articular cartilage and the effects of glycosidase treatments. *Journal of Orthopaedic Research*, *11*(6), pp.771-781.

[32] Bujia, J., Sittinger, M., Minuth, W.W., Hammer, C., Burmester, G. and Kastenbauer, E., 1995. Engineering of cartilage tissue using bioresorbable polymer fleeces and perfusion culture. *Acta Oto-laryngologica*, *115*(2), pp.307-310.

[33] Stading, M. and Langer, R., 1999. Mechanical shear properties of cell-polymer cartilage constructs. *Tissue Engineering*, *5*(3), pp.241-250.

[34] Wan, L.Q., Jiang, J., Miller, D.E., Guo, X.E., Mow, V.C. and Lu, H.H., 2011. Matrix deposition modulates the viscoelastic shear properties of hydrogel-based cartilage grafts. *Tissue Engineering Part A*, *17*(7-8), pp.1111-1122.

[35] Stammen, J.A., Williams, S., Ku, D.N. and Guldberg, R.E., 2001. Mechanical properties of a novel PVA hydrogel in shear and unconfined compression. *Biomaterials*, *22*(8), pp.799-806.

[36] Boere, K.W., Visser, J., Seyednejad, H., Rahimian, S., Gawlitta, D., Van Steenbergen, M.J., Dhert, W.J., Hennink, W.E., Vermonden, T. and Malda, J., 2014. Covalent attachment of a three-dimensionally printed thermoplast to a gelatin hydrogel for mechanically enhanced cartilage constructs. *Acta Biomaterialia*, *10*(6), pp.2602-2611.

[37] Moutos, F.T., Estes, B.T. and Guilak, F., 2010. Multifunctional hybrid three-dimensionally woven scaffolds for cartilage tissue engineering. *Macromolecular Bioscience*, *10*(11), pp.1355-1364.

[38] Wilson, W., Van Donkelaar, C.C., Van Rietbergen, B., Ito, K. and Huiskes, R., 2004. Stresses in the local collagen network of articular cartilage: a poroviscoelastic fibril-reinforced finite element study. *Journal of Biomechanics*, *37*(3), pp.357-366.

[39] Kääb, M.J., Ito, K., Clark, J.M. and Nötzli, H.P., 1998. Deformation of articular cartilage collagen structure under static and cyclic loading. *Journal of Orthopaedic Research*, *16*(6), pp.743-751.

[40] Li, L.P., Buschmann, M.D. and Shirazi-Adl, A., 2000. A fibril reinforced nonhomogeneous poroelastic model for articular cartilage: inhomogeneous response in unconfined compression. *Journal of Biomechanics*, *33*(12), pp.1533-1541.

[41] Chen, M.J., Kimpton, L.S., Whiteley, J.P., Castilho, M., Malda, J., Please, C.P., Waters, S.L. and Byrne, H.M., 2017. Multiscale modelling and homogenisation of fibre-reinforced hydrogels for tissue engineering. *European Journal of Applied Mathematics*, pp.1-29.

[42] Pence, T.J. and Gou, K., 2015. On compressible versions of the incompressible neo-Hookean material. *Mathematics and Mechanics of Solids*, *20*(2), pp.157-182.